Monthly Notices
of the
ROYAL ASTRONOMICAL SOCIETY

MNRAS **450,** 1279–1294 (2015) doi:10.1093/mnras/stv374

The UV, Lyman α, and dark matter halo properties of high-redshift galaxies

T. Garel,[1⋆†] J. Blaizot,[2] B. Guiderdoni,[2] L. Michel-Dansac,[2] M. Hayes[3] and A. Verhamme[4]

[1] *Centre for Astrophysics and Supercomputing, Swinburne University of Technology, Hawthorn, Victoria 3122, Australia*
[2] *Université de Lyon, Lyon, F-69003; Université Lyon 1, Observatoire de Lyon, 9 avenue Charles André, Saint-Genis Laval, F-69230; CNRS, UMR 5574, Centre de Recherche Astrophysique de Lyon; Ecole Normale Supérieure de Lyon, Lyon, F-69007, France*
[3] *Department of Astronomy, Oskar Klein Centre, Stockholm University, AlbaNova University Centre, SE-106 91 Stockholm, Sweden*
[4] *Observatoire de Genève, Université de Genève, 51, Ch. des Maillettes, CH-1290 Versoix, Switzerland*

Accepted 2015 February 19. Received 2015 January 27; in original form 2014 October 21

ABSTRACT

We explore the properties of high-redshift Lyman alpha emitters (LAEs), and their link with the Lyman-break galaxy (LBG) population, using a semi-analytic model of galaxy formation that takes into account resonant scattering of Lyα photons in gas outflows. We can reasonably reproduce the abundances of LAEs and LBGs from $z \approx 3$ to 7, as well as most UV luminosity functions (LFs) of LAEs. The stronger dust attenuation for (resonant) Lyα photons compared to UV continuum photons in bright LBGs provides a natural interpretation to the increase of the LAE fraction in LBG samples, $X_{\rm LAE}$, towards fainter magnitudes. The redshift evolution of $X_{\rm LAE}$ seems however very sensitive to UV magnitudes limits and equivalent width (EW) cuts. In spite of the apparent good match between the statistical properties predicted by the model and the observations, we find that the tail of the Lyα EW distribution (EW $\gtrsim 100$ Å) cannot be explained by our model, and we need to invoke additional mechanisms. We find that LAEs and LBGs span a very similar dynamical range, but bright LAEs are $\sim$4 times rarer than LBGs in massive haloes. Moreover, massive haloes mainly contain weak LAEs in our model, which might introduce a bias towards low-mass haloes in surveys which select sources with high-EW cuts. Overall, our results are consistent with the idea that LAEs and LBGs make a very similar galaxy population. Their apparent differences seem mainly due to EW selections, UV detection limits, and a decreasing Lyα to UV escape fraction ratio in high star formation rate galaxies.

Key words: radiative transfer – methods: numerical – galaxies: evolution – galaxies: formation – galaxies: high-redshift.

1 INTRODUCTION

Star-forming galaxies are commonly detected nowadays via two main channels at high redshift ($z \gtrsim 3$). On the one hand, the Lyman-break technique is quite efficient at selecting objects with strong stellar UV continuum ($\lambda \approx 1500$ Å), using a set of broad-band colour–colour criteria (e.g. Steidel et al. 1996, 1999, 2003; Gabasch et al. 2004; Bouwens et al. 2007, 2011). On the other hand, narrow-band (NB) imaging and spectroscopic surveys have also been able to probe large samples of high redshift sources via their (nebular) Lyα emission line ($\lambda = 1215.67$ Å; e.g. Hu, Cowie & McMahon 1998; Rhoads et al. 2000; Shimasaku et al. 2006; Ouchi et al. 2008; Rauch et al. 2008; Hayes et al. 2010; Hu et al. 2010; Blanc et al. 2011; Cassata et al. 2011).

The joint study of these two populations is essential to improve our understanding of the formation and evolution of galaxies in the early Universe, and their impact on the intergalactic gas notably during the epoch of reionization. Large observational data sets have enabled to constrain many statistical properties of Lyman-break galaxies (LBGs) and Lyman-alpha emitters (LAEs). The evolution of the UV luminosity function (LF) of dropout galaxies appears to be much stronger than the Lyα LF of LAEs at $z \approx 3$–7. In terms of physical properties, typical LBGs correspond to massive objects, with stellar mass correlated to UV luminosity (Shapley et al. 2001; Bouwens et al. 2010; González et al. 2011). LAEs are commonly thought to be less massive galaxies and to form a highly

⋆Australian Research Council Super Science Fellow.
†E-mail: tgarel@astro.swin.edu.au

inhomogeneous population in terms of age, mass or dust content (Gawiser et al. 2006; Finkelstein et al. 2007, 2009; Pirzkal et al. 2007; Ono et al. 2010). Although part of the difference between the LBG and LAE populations is inherent to their respective, both biased, methods of selection, their link is not quite well established yet, and it is still unclear to what extent they are representative of the underlying galaxy population.

In the modern picture of hierarchical structure formation, galaxies form through gas accretion within virialized haloes of dark matter located at the density peaks of the background matter field (Birnboim & Dekel 2003; Kereš et al. 2005; Dekel et al. 2009). The internal properties of galaxies are tightly linked to the characteristics of the host haloes. The host halo masses of typical LBGs are inferred to be one order of magnitude larger than those of currently observed LAEs from angular autocorrelation function measurements (Hamana et al. 2004; Gawiser et al. 2007; Hildebrandt et al. 2009; McLure et al. 2009; Ouchi et al. 2010) and halo occupation distribution models (Lee et al. 2006; Jose, Srianand & Subramanian 2013).

Accurate estimates on the halo masses of LBGs and LAEs at high redshift are crucial to constrain formation history of local galaxies and identify the progenitors of the Milky Way in the hierarchical context. The observed LBGs and LAEs luminosities span several orders of magnitude and their host halo properties are thus expected to cover a wide range. Although it is essential to investigate the connection between UV/Lyα-selected galaxies and their dark matter haloes within cosmological simulations, special care has first to be taken to describe the complex transfer of Lyα photons in the interstellar medium (ISM).

The line emission originates in H II regions in the ISM as ionizing radiation produced by massive, short-lived, stars is reprocessed into Lyα photons. The *intrinsic* Lyα emission is then a direct tracer of recent star formation (SF) activity in galaxies. However, the *observed* flux can be strongly reduced by dust extinction in the ISM and intervening hydrogen absorption in the intergalactic medium (IGM). Due to a large absorption cross-section combined with substantial H I column densities, the medium becomes optically thick to Lyα photons which undergo a resonant scattering process. Lyα photons diffuse both in frequency and physical space which can strongly alter the shape of the observed line. The travelling path in neutral gas, as well as the probability of encounter with dust grains, may be dramatically increased, and interactions with atoms in the tail of the velocity distribution can scatter photons off to the wing. Lyα radiation transfer (RT) is thus highly sensitive to the geometry, the ionization state, and the kinematics of the ISM.

Only very idealized cases can be investigated analytically (e.g. Neufeld 1990; Dijkstra, Haiman & Spaans 2006) and more realistic configurations require numerical schemes, mostly based on the Monte Carlo technique (Ahn, Lee & Lee 2001; Zheng & Miralda-Escudé 2002; Dijkstra et al. 2006; Hansen & Oh 2006; Verhamme, Schaerer & Maselli 2006; Laursen & Sommer-Larsen 2007; Laursen, Duval & Östlin 2013). Although a plethora of codes have been developed, only a few authors have intended to address the Lyα RT issue on galactic scales within hydrodynamical simulations (Tasitsiomi 2006; Laursen, Sommer-Larsen & Andersen 2009; Barnes et al. 2011; Verhamme et al. 2012; Yajima et al. 2012). These studies are extremely useful because they can follow the propagation of Lyα photons through more realistic, non-linear, ISM density/velocity fields. Even though some trends are identified (anticorrelation between halo mass and Lyα escape fraction, orientation effects, etc.), the results still appear to depend on the resolution and the physics implemented in the underlying hydrodynamical simulation (e.g. Verhamme et al. 2012). Moreover, only a handful of high-resolution galaxies can be studied at once due to computing time issues.

Semi-analytic models (SAM) of galaxy formation provide a unique alternative to investigate statistical samples of mock galaxies and their evolution with redshift. Recently, several models accounting for the Lyα RT in galaxies based on numerical libraries have been presented. Rather simplistic physical pictures are usually adopted, such as plane-parallel slab geometries (Forero-Romero et al. 2011) or thin expanding shell models (Garel et al. 2012; Orsi, Lacey & Baugh 2012). None the less, these approaches provide a more accurate treatment than previous models which used simple parametrizations to describe the Lyα transfer effects and the *observed* Lyα properties of galaxies, assuming a constant Lyα escape fraction (e.g. Le Delliou et al. 2005; Nagamine et al. 2010), simple dust models neglecting Lyα resonant scattering (Mao et al. 2007), or using phenomenological prescriptions to account for its effect (Kobayashi, Totani & Nagashima 2007, 2010; Dayal, Maselli & Ferrara 2011).

In this paper, we use the SAM presented in Garel et al. (2012) to investigate the UV, Lyα, and dark matter haloes properties of high-redshift galaxies. In Garel et al. (2012, hereafter Paper I), we described the coupling of GALICS (GALaxies In Cosmological Simulations; Hatton et al. 2003), a hybrid model of galaxy formation based on an *N*-body cosmological simulation, with the library of Schaerer et al. (2011a) which computes numerically the Lyα RT through expanding gas shells. We present an overview of our model in Section 2. In Section 3, we show that this model is able to reproduce the observed UV and Lyα LFs from $z \approx 3$ to $z \approx 7$. In Sections 4 and 5, we investigate the observed cross-properties of LAEs and LBGs to study the connection between these two populations, focusing on the Lyα equivalent width (EW) distributions. In Section 6, we present our model predictions for the host halo properties of LAEs and LBGs in terms of halo mass and occupation number. Finally, Section 7 gives a discussion and a summary of our results.

All quantities used throughout this paper assume the following cosmological parameter values: $h = H_0/(100\,\mathrm{km\,s^{-1}\,Mpc^{-1}}) = 0.70$, $\Omega_\Lambda = 0.72$, $\Omega_\mathrm{m} = 0.28$, $\Omega_\mathrm{b} = 0.046$, and $\sigma_8 = 0.82$ (*WMAP*-5; Komatsu et al. 2009). All magnitudes are expressed in the AB system.

2 MODEL OVERVIEW

Our modelling of the high-redshift galaxies and their Lyα emission properties has been fully described in Paper I. Here, we briefly summarize the main aspects of our approach.

We use an updated version of the GALICS semi-analytic galaxy formation model to predict the abundances and physical properties of galaxies, based on the hierarchical evolution of dark matter haloes. The formation and evolution of dark matter structures is described by a cosmological *N*-body simulation post-processed with a Friends-of-Friends algorithm (Davis et al. 1985) to identify bound regions (i.e. dark matter haloes). The merging histories of dark matter haloes are computed according to the procedure of Tweed et al. (2009). Our *N*-body simulation has been run with GADGET (Springel 2005) using 1024^3 particles in a periodic, comoving box of $100\,h^{-1}$ Mpc on a side. The mass resolution ($M_\mathrm{halo} \geq 2 \times 10^9\,\mathrm{M}_\odot$, corresponding to bound groups of at least 20 particles) and the box size have been chosen to allow us to investigate the statistical properties of LAEs and LBGs currently detectable at high redshift. While in Paper I we assumed parameter values from the *WMAP*-3

release (Spergel et al. 2007), here we adopt a more recent set of cosmological parameters consistent with the *WMAP*-5 data, which are described above.

Our modelling of galaxies and Lyα emission is very similar to Paper I, except for a few changes that we detail below. In Paper I, we presented the modifications made to the original GALICS model described in Hatton et al. (2003, see also Cattaneo et al. 2006). The main updates consisted of a new implementation of gas accretion on to galaxies (cold flows), dust extinction of the UV continuum (spherical geometry so as to be consistent with the Lyα radiative transfer within outflowing shells of gas – see below), and SF. We compute star formation rates (SFRs) directly from the cold gas surface density using the Kennicutt–Schmidt law (i.e. $\Sigma_{\rm SFR} \propto \Sigma_{\rm gas}^{1.4}$), and we had to increase the SF efficiency by a factor of 25 in order to match the observed high-redshift UV LFs. This departure from the $z = 0$ normalization of Kennicutt (1998) was certainly due to the underlying (*WMAP*-3) cosmology that we adopted for the dark matter simulation, and especially the low value of σ_8 (0.76; Spergel et al. 2007) which delays the growth of structure at early times. To this extent, boosting SF was necessary to compensate the low abundance of star-forming galaxies at high redshift. With our new N-body simulation, σ_8 is slightly higher which eases the formation of larger structures at earlier epochs. We find that an increasing factor for a SF efficiency equal to 5 in our model is sufficient to obtain a reasonable match to the high-redshift data (see Section 3).

We use the stellar libraries of Devriendt, Guiderdoni & Sadat (1999, STARDUST) to compute the intrinsic UV and Lyα emission of galaxies for a Kennicutt IMF (0.1–120 $M_\odot$; Kennicutt 1983). Under the case B approximation (Osterbrock & Ferland 2006), two-third of the ionizing photons emitted by stars are reprocessed into Lyα photons when H II regions recombine, and we assume that no ionizing photon can escape the medium (optically thick limit).The intrinsic Lyα luminosity of galaxies is therefore given by $L_{\rm Ly\alpha}^{\rm intr} = 0.67 Q({\rm H}) \frac{h_{\rm P} c}{\lambda_\alpha}$, where Q(H) is the production rate of hydrogen-ionizing photons, c the speed of light, $h_{\rm P}$ the Planck constant, and λ_α is the Lyα wavelength at line centre. For the shape of the intrinsic line, we assume a Gaussian profile centred on λ_α with a characteristic width given by the circular velocity of the galaxy disc (Santos 2004).

We take into account the transfer of UV continuum and Lyα radiation through outflowing gas and dust. This picture is motivated by the apparent ubiquity of galactic winds seen at high redshift (powered by supernovae and/or stellar winds), as well as their impact on the observed Lyα spectral signature in LBGs and LAEs (Shapley et al. 2003; Steidel et al. 2010; Finkelstein et al. 2011; McLinden et al. 2011; Berry et al. 2012; Kulas et al. 2012). Following the work of Verhamme et al. (2006), we describe galactic outflows as homogenous, spherical, expanding shells of cold gas mixed with dust. Verhamme et al. (2008) have shown that high-redshift Lyα line profiles can be well reproduced by 3D Monte Carlo RT models in expanding shells, when adjusting the values of various relevant shell parameters: the bulk motion expansion velocity $V_{\rm exp}$, the gas velocity dispersion b, the dust opacity $\tau_{\rm dust}$, and the neutral hydrogen column density of the shell $N_{\rm H\,I}$. We compute shell parameters for GALICS galaxies in a similar fashion to Paper I. In our model, the shell speed $V_{\rm exp}$ has a (weak) dependence on the SFR, the value of b is fixed to 20 km s^{-1}, and the dust opacity is estimated from the Mathis, Mezger & Panagia (1983) extinction curve at a given wavelength, the gas metallicity and column density, and a redshift-dependent dust-to-gas ratio (see Paper I for a detailed description of our model). The column density is proportional to $M_{\rm shell}^{\rm gas}/(4\pi {R_{\rm shell}}^2)$, where $M_{\rm shell}^{\rm gas}$ and $R_{\rm shell}$ are the shell mass and size, respectively. We use the cold gas in galaxies as a proxy for the shell mass, and the disc scalelength $R_{\rm disc}$ to compute $R_{\rm shell}$ such that $R_{\rm shell} = \xi R_{\rm disc}$ where ξ is a free parameter of the order of unity. While ξ was 1.0 in Paper I, we now set the value to 1.2 to improve the agreement of our model with the LFs data over our redshift range of interest.

The escape fraction of UV continuum photons is $e^{-\tau_{\rm dust}}$, as for a screen model, consistent with the thin shell approximation we make here. On the other hand, we predict the Lyα properties of galaxies using the grid of models of Schaerer et al. (2011a) which contains the results of a large number of Lyα RT simulations in expanding shells, as described above (see Verhamme et al. 2006, for more details). The grid provides us with the Lyα escape fraction $f_{\rm esc}^{\rm grid}$ and the emergent line profile $\Phi^{\rm grid}$(Lyα) for more than 6000 quadruplets of parameter values ($V_{\rm exp}$, b, $\tau_{\rm dust}$, $N_{\rm H\,I}$). We interpolate the shell parameters predicted by GALICS on to the grid so as to compute $f_{\rm esc}$ and Φ(Lyα) for each individual galaxy. The *observed* Lyα luminosities are thus given by $L_{\rm Ly\alpha} = L_{\rm Ly\alpha}^{\rm intr} \times f_{\rm esc}$.

A main result of this modelling is that $f_{\rm esc}$ is of the order of unity for galaxies with a low star formation rate (SFR $\lesssim 1\,M_\odot\,{\rm yr}^{-1}$) because they are predicted to have low gas column densities and dust opacities (see section 3.2.3 in Paper I). This suggests that the observed Lyα luminosity could be used on average as a tracer of the SFR for faint LAEs. On the other hand, $f_{\rm esc}$ is greatly dispersed between 0 and 1 for high-SFR galaxies because star forming galaxies can have a wide range of $N_{\rm H\,I}$ and $\tau_{\rm dust}$ values in our model. For these galaxies, Lyα is no longer a reliable tracer of the SFR.

Our model only assumes the internal attenuation of the Lyα line by dust in the shell, and the effect of the IGM is neglected. We will discuss this choice in more details in Section 3.2.

3 ABUNDANCES OF LBGs AND LAEs

In this section, we present the UV and Lyα LFs at $z = 3$–7, a redshift range that corresponds to the post-reionization epoch where most dropout galaxy and LAE surveys have been conducted so far.

3.1 UV LFs

Observationally, rest-frame UV LF are now rather well constrained up to $z \approx 6$. At higher redshift, significant scatter in the data remains, mainly due to smaller statistics, larger cosmic variance effects, and more numerous contamination by foreground sources. In Fig. 1, we show the UV LFs at $z \approx 3$, 4, 5, 6, 7, and 7.5. In each panel, the solid black line corresponds to the LF with dust attenuation, and the dashed curve gives the intrinsic LF, i.e. without dust attenuation. The observations, represented by the symbols with error bars, come from various surveys of LBGs.

Overall, our model provides a good fit to the data over the redshift range of interest. While we note some tension at the faint end of the $z = 3$ LF, the agreement between the model and the observations is excellent at these magnitudes for $z = 4$ and 5. We somehow underpredict the luminosities and/or number densities of dropout galaxies at $z = 7.5$ (bottom-right panel in Fig. 1). Given that the intrinsic LF agrees with the data, our modelling of dust attenuation is perhaps too strong at $z = 7.5$. We do not think of this small mismatch between the model and the observations as a real issue since the observed UV LF is still uncertain at this redshift (as the fraction of interlopers could be quite high in $z = 7$–8 samples of dropout galaxies).

The LBG selection probes bright UV-continuum sources (at ∼1300–1700 Å in rest frame) and applies colour–colour criteria

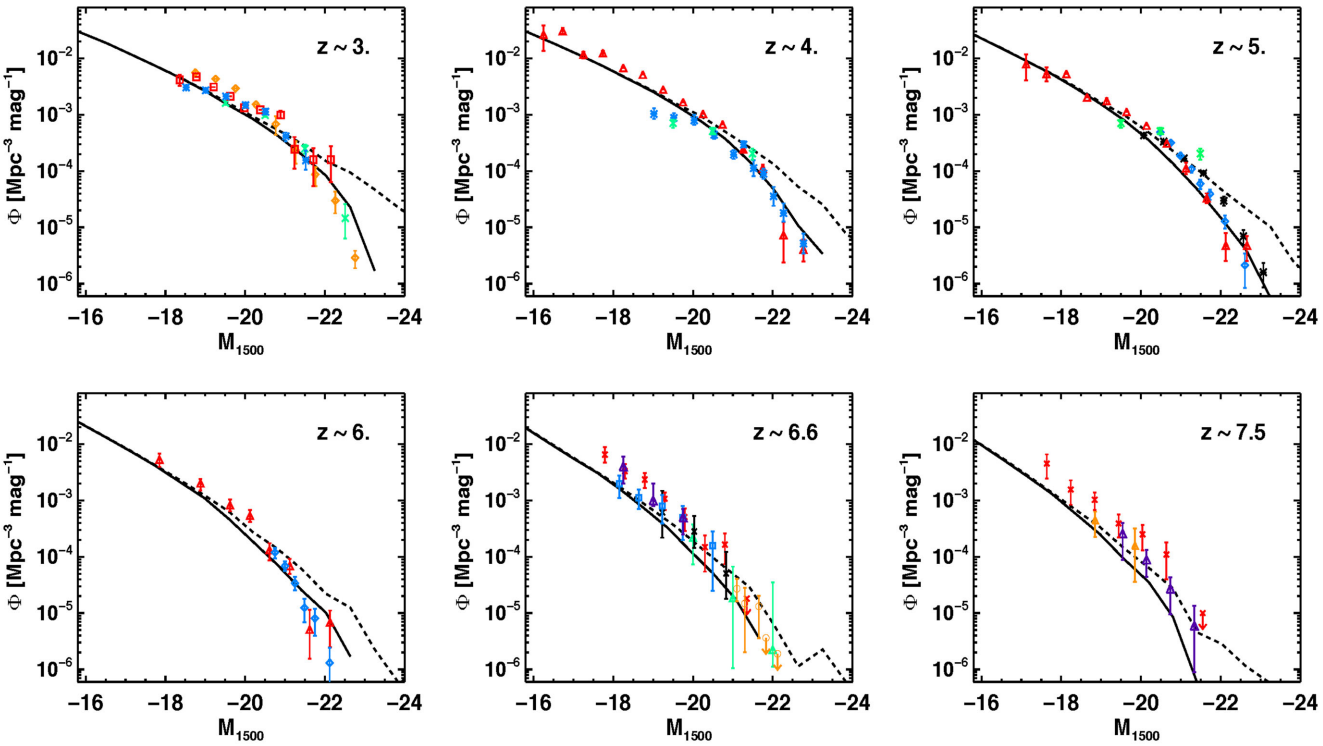

Figure 1. UV LFs at $z \approx 3$, 4, 5, 6, 7, and 7.5. The solid (dashed) line is the model with (without, i.e. intrinsic) dust extinction. Symbols are observational data: Reddy et al. (2008, orange diamonds), Arnouts et al. (2005, red squares), Sawicki & Thompson (2006, blue asterisks), Gabasch et al. (2004, green crosses), Bouwens et al. (2007, red triangles), Iwata et al. (2007, black asterisks), McLure et al. (2009, blue diamonds), Castellano et al. (2010, light green triangles), Bouwens et al. (2011, red crosses), Bouwens et al. (2008, black crosses), McLure et al. (2010, blue squares), Ouchi et al. (2009, orange circles), Oesch et al. (2010, 2012, purple triangles).

to ensure the detections at a given redshift, minimizing the contamination by interlopers. The selection and filters vary from one survey to another, so, in our model, we choose to directly measure the rest-frame absolute UV magnitude of galaxies in an effective rectangular filter at 1500 ± 100 Å to compute the UV LF (as quoted by Gabasch et al. 2004), without any colour–colour selection. These different selections only introduce a little variation on the UV LFs but they could still be responsible for part of the slight differences seen in the LFs between the various surveys, and between the data and the model.

3.2 Lyα LFs

In comparison to UV LFs, the Lyα LFs are computed observationally over smaller samples so cosmic variance effects remain significant. Moreover, most LAEs are detected using the NB technique which introduces a selection in Lyα EW.[1] The Lyα LFs are therefore computed over EW-limited samples that are not complete in terms of Lyα luminosity, so caution must be taken when comparing LFs from various surveys which select LAEs differently (i.e. with different EW cuts).

In Fig. 2, we compare the Lyα LF from our model with available observational data at six redshifts ($z = 3$, 3.7, 4.7, 5.7, 6.5, and 7). To build the LFs, we only consider the Lyα luminosity of galaxies, and, unlike observations (symbols with error bars), we do not apply any EW thresholds. Hence, we expect our LFs to lie above data points which come from LAE samples selected with high-EW thresholds. For instance, Ouchi et al. (2008, 2010) obtained four NB-selected samples of LAEs at $z \approx 3.1$, 3.7, 5.7, and 6.6, which are often taken as a reference to study the statistical properties of LAEs, and notably the evolution of Lyα LF, given the rather large number of objects contained in their samples (a few hundreds at each redshift). In these surveys, the selection of LAEs implied EW thresholds which decline with increasing redshift (i.e. 64, 44, 27, and 14 Å at $z = 3.1$, 3.7, 5.7, and 6.6, respectively), and it is unclear how this selection effect affects our interpretation of the redshift evolution of the LAE population. Especially, the EW threshold of 64 Å at $z = 3.1$ coincides with the typical EW value predicted for galaxies with constant SF (Charlot & Fall 1993). Then, a significant fraction of LAEs can possibly be missed with such observational threshold.

From Fig. 2, we first note that the overall agreement is quite acceptable given the complexity of the mechanisms involved in the Lyα transfer, and the simplicity of the physical picture we assume in this paper. Especially, our LFs compare very well to the observed ones at $z \approx 3.7$ and 4.7 (top centre and right-hand panels in Fig. 2). At $z \approx 3$ (top-left panel), although our model agrees well with the spectroscopic data of Blanc et al. (2011) and van Breukelen et al. (2005) at $L_{\mathrm{Ly}\alpha} \gtrsim 10^{42}$ erg s^{-1} (blue asterisks and red diamonds, respectively), it overpredicts by a factor of ∼1.5–2 the number density reported by Ouchi et al. (2008, green squares). As already discussed in Paper I, our LF can be reconciled with their data if we impose high-EW cuts ($\mathrm{EW}_{\mathrm{Ly}\alpha} \gtrsim 50$ Å provides the best match).

At the faint end of the LF, our predictions seem to favour the number density reported by Rauch et al. (2008). These observations are however in slight disagreement with the findings of Cassata

[1] All EW values discussed in this paper are rest-frame EWs.

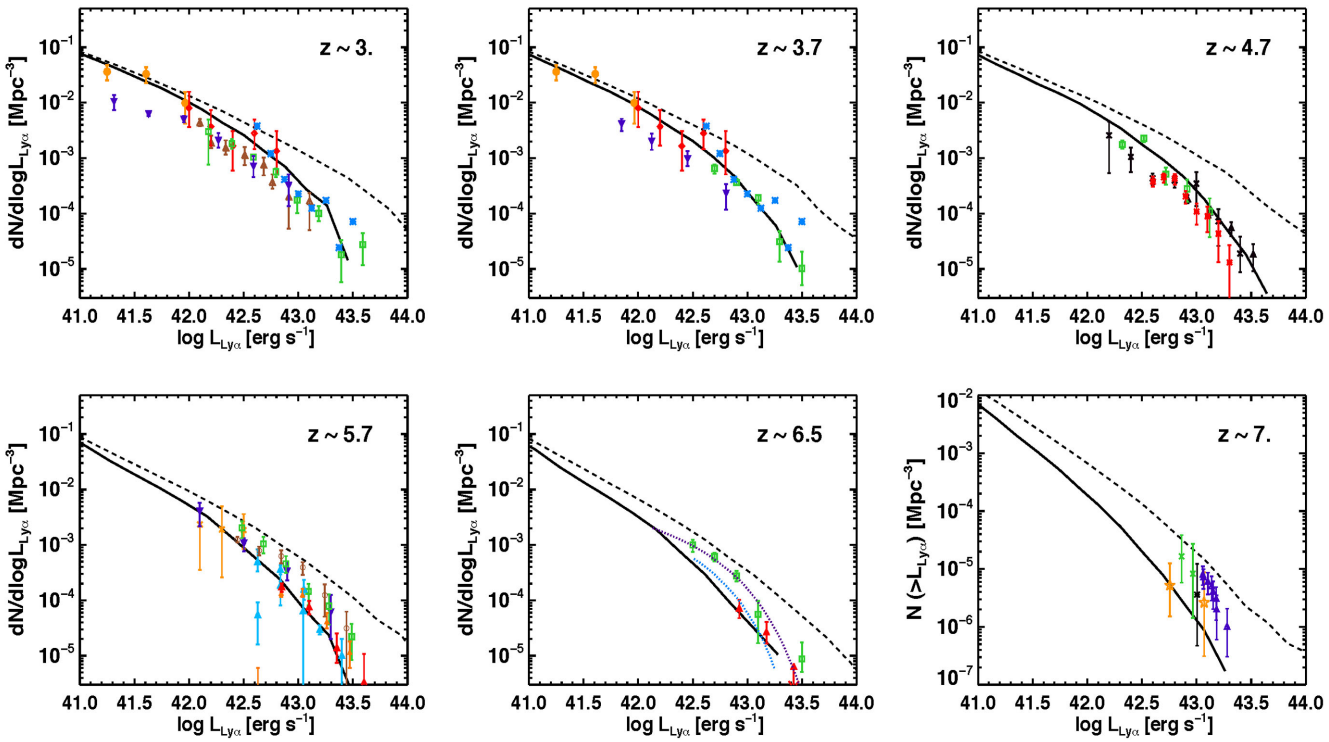

Figure 2. Lyα LFs at $z \approx 3$, 3.7, 4.7, 5.7, 6.5, and 7. The solid (dashed) line is the model with (without, i.e. intrinsic) dust. Symbols are observational data from van Breukelen, Jarvis & Venemans (2005, red diamonds, $2.3 < z < 4.6$), Gronwall et al. (2007, brown triangles, $z = 3.1$), Ouchi et al. (2003, 2008, 2010, green squares, $z = 3.1$, 3.7, 4.9, 5.7 and 6.6), Blanc et al. (2011, blue asterisks, $2.8 < z < 3.8$), Rauch et al. (2008, orange circles, $2.67 < z < 3.75$), Cassata et al. (2011, purple downward triangles, $z \approx 3$, 4, 6), Dawson et al. (2007, black crosses, $z = 4.5$), Wang et al. (2009, red asterisks, $z = 4.5$), Shioya et al. (2009, black triangles, $z = 4.9$), Henry et al. (2012, orange crosses, $z = 5.7$), Shimasaku et al. (2006, brown circles, $z = 5.7$), Hu et al. (2010, red triangles, $z = 5.7$ and 6.6), Ajiki et al. (2003, 2004, 2006, light blue triangles, $z = 5.7$), Murayama et al. (2007, orange triangles, $z = 5.7$), Malhotra & Rhoads (2004, blue dotted line, $z = 6.5$), Kashikawa et al. (2011, purple dotted line, $z = 6.5$), Shibuya et al. (2012, orange stars, $z \approx 7$), Hibon et al. (2012, purple triangles, $z \approx 7$), Iye et al. (2006, black asterisk, $z \approx 7$) and Vanzella et al. (2011, green crosses, $z \approx 7$).

et al. (2011) who measure a density of LAEs a few times lower for a similar detection limit ($L_{Ly\alpha} \gtrsim 10^{41}$ erg s^{-1} at $z \approx 3$). Cosmic variance effects, due to the rather small and elongated volumes that are probed, as well as incompleteness issues or slit losses may explain the discrepancy between both measurements. Larger homogeneous data sets are therefore still needed to better constrain the Lyα LF at the faint end. This will be one of the key objectives of forthcoming instruments like the Multi Unit Spectrograph Explorer (MUSE; Bacon et al. 2006) which recently started to operate at VLT. We will address these issues in more details in a next paper (Garel et al., in preparation).

At $z \approx 5.7$ and 6.5, the EW cuts employed in NB surveys are small (≈15–25 Å) so the impact on the selection of LAEs should be minor. As can be seen from Fig. 2, the shape and the normalization of the observed Lyα LF at $z \approx 5.7$ and 6.5 varies significantly from one survey to another, and our model agrees better with the lower end of the envelope of data points. For instance, at $z \approx 6.5$, while our model reproduces nicely the observed LFs of Hu et al. (2010, red diamonds in Fig. 2), it underpredicts by a factor of 2–4 the number densities of Ouchi et al. (2008, 2010, green squares) and Kashikawa et al. (2011, purple dotted line). The LF of Hu et al. (2010) was computed from their spectroscopic sample and they find that only ≈50 per cent of the LAE candidates could be confirmed by spectroscopy. To explain the difference between the LFs, Hu et al. (2010) argue that the photometric samples of Ouchi et al. (2010) might contain high fractions of interlopers. However, Kashikawa et al. (2011) report that the rate of contamination in the photometric sample of Taniguchi et al. (2005) at $z \approx 6.5$ is less than 20 per cent, and their LF is in much better agreement with the results of Ouchi et al. (2010) than those of Hu et al. (2010). Kashikawa et al. (2011) claim that the difference may come from the lack of completeness at the faint end in the sample of Hu et al. (2010), due to the shallow depth of their spectroscopic follow-up survey.

Therefore, we conclude that our model is in agreement with observations at $z \gtrsim 6$ only when comparing with the data that report the lowest densities of sources at the bright end of the LF. A weaker of effect of dust, or higher intrinsic Lyα luminosities would be required to match the data of Ouchi et al. (2010) or Kashikawa et al. (2011).

We note that we do not take the effect of the IGM into account in our model whereas it is well known that neutral hydrogen atoms can scatter photons on the blue side of the Lyα resonance off the line of sight. This could strongly reduce the transmitted Lyα flux, especially at $z \gtrsim 6$. However, as already shown by e.g. Santos (2004) and Dijkstra & Wyithe (2010), Lyα radiative transfer through gas outflows can Doppler-shift Lyα photons towards longer wavelengths and then considerably reduce the impact of IGM. In Paper I (section 4.4), we used the prescription of Madau (1995) to compute the mean contribution of the Lyα forest as a function of redshift. We showed that the IGM had a negligible impact on the Lyα luminosities of galaxies in our model up to $z \approx 5$ because of the peak of the Lyα lines being redshifted sufficiently away from line centre by the scattering in the expanding shells. Here, we did a similar test, and we found that the Lyα LFs up to redshift 7 remain unaffected by

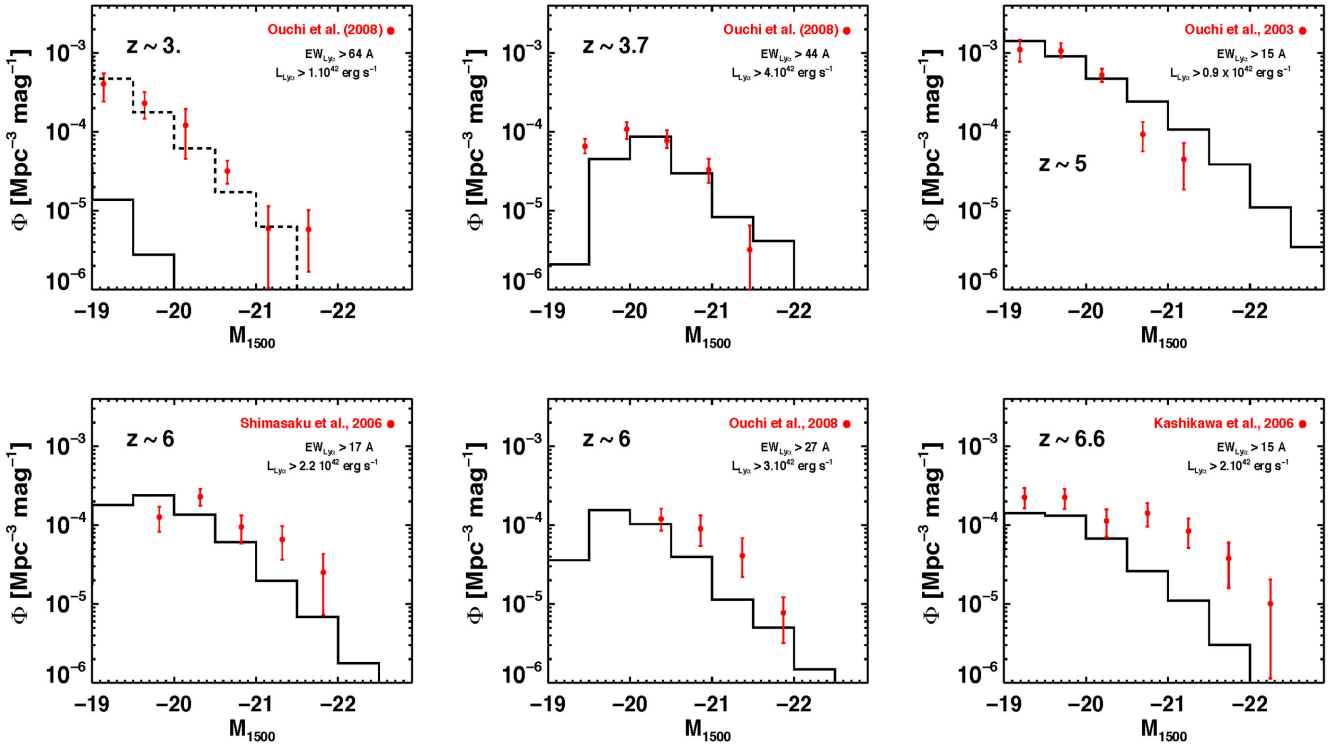

Figure 3. UV LFs of Lyα-selected galaxies at $z \approx 3$, 3.7, 5, 6, and 6.6. The solid lines correspond to the model with dust attenuation included and the red filled circles are observational data (Ouchi et al. 2003, 2008; Kashikawa et al. 2006; Shimasaku et al. 2006). We compared our model to each data set individually, applying selections in terms of Lyα luminosities and EW so as to mimic real observations (see legends). The dashed line in the top-left panel corresponds to a selection where the EW threshold of Ouchi et al. (2008) has been decreased from 64 to 50 Å. With such a small change (≈20 per cent), our model agrees quite well with the data.

the IGM transmission, for the same reasons as explained above. We also tested the recent model of Inoue et al. (2014) which predicts a slightly higher (lower) Lyα transmission at $z \lesssim 4.7$ ($z \gtrsim 4.7$) than the recipe of Madau (1995), and gives a better fit to the observational data. Again, as the Lyα lines of most our galaxies are Doppler-shifted, this IGM attenuation model has also almost no effect on the Lyα fluxes at all redshifts.. Nevertheless, we note that Laursen, Sommer-Larsen & Razoumov (2011) have shown that the IGM can non-negligibly reduce the flux on the red side of the Lyα line at $z \gtrsim 6$. Moreover, additional contributions to the IGM opacity might be important at $z \gtrsim 6$, such as (i) the potential high number density of Lyman-limit systems (Bolton & Haehnelt 2012), or (ii) the increasing neutral fraction of the diffuse component of the IGM, $x_{\rm H\,I}$, before reionization is fully complete (see Dijkstra 2014, for more details). Thus, a more refined IGM model with full RT treatment would be needed to assess the exact effect of the IGM on the Lyα lines in our model.

The end of the epoch of reionization is still a subject of debate, and the value of $x_{\rm H\,I}$ at $z = 6$–7 is not fully constrained yet (e.g. Dijkstra 2014). In addition, Lyα observations are often used as a probe of $x_{\rm H\,I}$, e.g. by measuring the evolution of the Lyα LF (Ouchi et al. 2010). In this context, it is interesting to note that our model intrinsically predicts a decrease of 50 per cent of the number density of bright LAEs at $L_{{\rm Ly}\alpha} = 10^{43}$ erg s^{-1} between $z = 5.7$ and 6.5 without accounting for the effect of IGM (Fig. 2).

We now turn our interest to the cross UV/Lyα properties of the LBG and LAE populations to study their link with one another. Owing to different methods of selection, the dropout and NB techniques do not necessarily probe the same galaxies, but both populations are a subset of a common parent population, and it is worth asking how they overlap.

4 UV/LYα PROPERTIES OF LAEs

4.1 The UV LFs of LAEs

Here, we compute the UV LFs of LAEs selected using Lyα luminosity and EW thresholds similar to various NB surveys (Fig. 3). In practice, we allow the observational cuts to vary by $\lesssim$20 per cent in order to improve the agreement with the data. This is justified by the fact that the quoted Lyα luminosity and EW thresholds do not exactly mimic the actual colour–magnitude selections (Ouchi et al. 2008; Dijkstra & Wyithe 2012).

Our model reproduces the UV LF of LAEs from Ouchi et al. (2008) and Ouchi et al. (2003) at $z \approx 3.7$ and 4.9, respectively, using selections similar to those reported by these authors (top centre and top-right panels in Fig. 3). At $z \gtrsim 6$, our model reproduces correctly the shape of the LFs observed by Ouchi et al. (2008), Shimasaku et al. (2006) and Kashikawa et al. (2006) but the overall normalization is somehow too low. Varying the Lyα luminosity and EW threshold has little effects because the cuts are low enough such that few galaxies with $M_{1500} < -18$ are removed by the Lyα selection. As for the comparison of our Lyα LFs with the data from the same surveys, it is plausible that the number density measured from photometric samples in these observations is overestimated due to non-negligible fractions of contaminants.

At $z \approx 3.1$ however, the observed LF is strongly underestimated if we use the EW threshold of Ouchi et al. (2008), as shown by the

solid histogram in the top-left panel. The value of 64 Å assumed by these authors is close to the median Lyα EW in our model, hence a large fraction of galaxies are below this selection limit. We need to decrease the EW threshold from 64 to 50 Å to bring the model into agreement with the data (dotted line in the top-left panel of Fig. 3). In other terms, at a given UV magnitude, the Lyα luminosities predicted by our model are not high enough compared to the LAEs of Ouchi et al. (2008). In the next section, we investigate the correlation between UV and Lyα emission in more details, and we quantitatively discuss plausible causes for the missing high EWs in the model.

4.2 Expected relation between intrinsic Lyα and UV emission

Assuming that SF is at the origin of all the Lyα and UV emission of galaxies, the relation between SFR and the intrinsic Lyα luminosity writes $L_{\mathrm{Ly}\alpha} = 1.2 \times 10^{42} (\mathrm{SFR}/\mathrm{M}_{\odot}\ \mathrm{yr}^{-1})\ \mathrm{erg\ s}^{-1}$ (Kennicutt 1998; Osterbrock & Ferland 2006). Following Madau, Pozzetti & Dickinson (1998), the relation between SFR and UV luminosity density evaluated at 1500 Å is $L_{\lambda,\mathrm{UV}} = 1.4 \times 10^{40} (\mathrm{SFR}/\mathrm{M}_{\odot}\ \mathrm{yr}^{-1})\ \mathrm{erg\ s}^{-1}\ \text{Å}^{-1}$.

Combining these formulae, $L_{\mathrm{Ly}\alpha}$ and M_{1500} scale with one another as follows:[2]

$$M_{1500} = -2.5 \log_{10} \left(\frac{L_{\mathrm{Ly}\alpha}}{10^{42}\ \mathrm{erg\ s}^{-1}} \right) - 18.3. \quad (1)$$

In this framework, galaxies with intrinsic luminosities of $L_{\mathrm{Ly}\alpha} = 10^{41}$, 10^{42} and 10^{43} erg s^{-1} should display $M_{1500} = -15.8$, -18.3 and -20.8, corresponding to SFRs of $\sim$0.08, 0.8 and 8 $\mathrm{M}_{\odot}\ \mathrm{yr}^{-1}$, respectively.

In Fig. 4, we investigate the relation between Lyα luminosity and UV magnitude at $z \approx 3$. In the upper panel, the distribution of galaxies from the model, represented by the black contours, shows the relation between Lyα luminosity and UV magnitude after the effect of dust. Overlaid are measurements from two sets of NB-selected LAEs. The cloud of data points from Gronwall et al. (2007, blue diamonds) covers a similar region to the model above their detection limit ($\approx 1.2 \times 10^{42}$ erg s^{-1}; blue dotted line). We note however that some data points lie above the model, i.e. their Lyα luminosity is larger than predicted by the model for a given UV magnitude. Now comparing with data of Ouchi et al. (2008, red crosses), we see this time that many LAEs lie above the model predictions. These objects belong to the tail of the Lyα EW distribution, that is EW $\gtrsim$ 100 Å, which our model does not reproduce. Moreover, we note that most LAEs from the survey of Ouchi et al. (2008) are above the ones of Gronwall et al. (2007) in the $L_{\mathrm{Ly}\alpha}$–M_{1500} plane, which is due to very different EW thresholds used to select LAEs (20 Å versus 64 Å).

In the middle panel of Fig. 4, we now show the model distribution of galaxies before applying the effect of dust. To show how the Lyα and UV intrinsic luminosities relation are expected to scale with one another as a function Lyα EW, we overplot the expected intrinsic $L^{\mathrm{intr}}_{\mathrm{Ly}\alpha}$–$M^{\mathrm{intr}}_{1500}$ relation for various EWs (as labelled on the plot), according to

$$\mathrm{EW}_{\mathrm{exp}} = \frac{L_{\mathrm{Ly}\alpha}}{L_{\lambda,\mathrm{UV}}} \left(\frac{\lambda_{\mathrm{UV}}}{\lambda_{\mathrm{Ly}\alpha}} \right)^{\beta}, \quad (2)$$

[2] These scaling relations assume a Kennicutt IMF, solar metallicity, the production of Lyα photons through Case B recombination at $T = 10^4$ K, and are valid for constant SF.

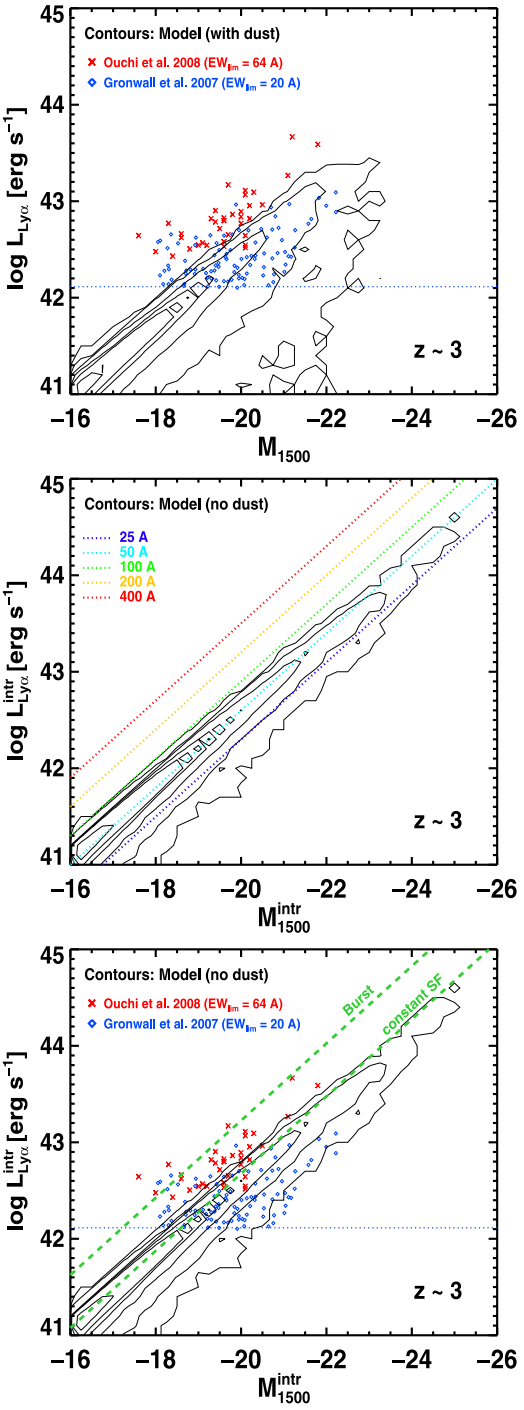

Figure 4. Distribution of LAEs in the Lyα luminosity versus UV magnitude plane at $z \approx 3$. The black contours show the number distribution of objects in the model (without any Lyα luminosity or EW cut). Top: Lyα luminosity versus UV magnitude (with dust attenuation included). The data of Gronwall et al. (2007, blue diamonds) and Ouchi et al. (2008, red crosses) are also shown. The blue dotted line show the Lyα detection limit of Gronwall et al. (2007). Middle: intrinsic Lyα luminosity versus intrinsic UV magnitude (without dust attenuation included). Overlaid are the expected relations for various Lyα EWs, according to equation (2). Bottom: intrinsic Lyα luminosity versus intrinsic UV magnitude (without dust attenuation included). The green dashed lines show the expected relation in the case of constant SF (equation 1), and in the case of an instantaneous starburst (see text). Same data as above (i.e. not corrected for dust).

where β is the UV slope used to renormalize the continuum luminosity density around the Lyα line. Here, we have assumed $\beta = -1.5$, which is a typical value for observed LAEs (e.g. Venemans et al. 2005; Blanc et al. 2011).

From the bottom panel of Fig. 4, it is obvious that many sources from the samples of Gronwall et al. (2007) and Ouchi et al. (2008) have observed EW larger than in the model, even before taking the effect of dust into account (contours). At the same time, we note that the relation between intrinsic Lyα luminosity and UV magnitude agrees well with the formula for constant SF from equation (1) (dashed green line). The production rate of Lyα photons, dominated by short-lived hot stars, traces the very recent SF, so the intrinsic Lyα luminosity, $L^{\rm intr}_{{\rm Ly}\alpha}$, is proportional to the SFR averaged over the last $\approx$10 Myr, (SFR($t \approx 10$ Myr); Charlot & Fall 1993). The UV continuum intensity is however a direct function of the mean SFR over longer time-scales, of the order of a few hundreds Myr ($L_{\lambda,\,{\rm UV}} \propto$ SFR($t \approx 100$ Myr); Madau et al. 1998). In the constant SF scenario, i.e. SFR($t \approx 10$ Myr) = SFR($t \approx 100$ Myr), the Lyα EW reaches an equilibrium value of approximatively 60 Å after $\approx$ 10 Myr, which is consistent with the median intrinsic EW value we find in our model.

In GALICS, SF is iteratively computed at each timestep using the Kennicutt law, namely $\Sigma_{\rm SFR} \propto \Sigma_{\rm gas}^{1.4}$, and a gas surface density threshold: $\Sigma_{\rm gas}^{\rm thresh} = 10^{21}$ cm^{-2}. This threshold, inferred from late-type galaxies observations, is in broad agreement with the Toomre model for gravitational instability-triggered SF (Kennicutt 1989). In GALICS, this criterion is met most of the time in LAEs and LBGs we consider in this paper, hence the SF appears to be close to a constant process, although there is scatter in the $L^{\rm intr}_{{\rm Ly}\alpha}$–$M^{\rm intr}_{1500}$ relation due to small variations of the recent SF history or stellar metallicity. We also consider here the $L^{\rm intr}_{{\rm Ly}\alpha}$–$M^{\rm intr}_{1500}$ relation (see fig. 15 of Verhamme et al. 2008) that is expected a few Myr after a burst of SF (dashed green line). We see from the bottom panel of Fig. 4 that the high-EW sources of Ouchi et al. (2008) can be interpreted by this scenario, which produces higher Lyα luminosity for a given UV emission than ongoing constant SF. Thus, the high-EW LAE population probed by Ouchi et al. (2008) could correspond to starburst galaxies, rather than constantly star-forming objects.

Although our model can recover the standard Lyα EWs (EW $\sim$ 0–70 Å) which seem to make the bulk of the LAE population (Cassata et al. 2011), it certainly requires extra ingredients to explain the high-EW galaxies.[3]

4.3 High Lyα EWs

As discussed in the previous section, the commonly observed of high-EW LAEs (EW $\gtrsim$ 100 Å) are missing in our model, even when considering intrinsic values. Here, we discuss various potential causes responsible for this mismatch.

First, it is often claimed that Lyα RT effects could enhance the intrinsic EW, as predicted by the analytic model of Neufeld (1991) for a multiphase medium. Laursen et al. (2013) and Duval et al. (2014) have shown that the (angle-averaged) boost of Lyα EWs in a clumpy multiphase medium would require very special conditions unlikely to exist in most high-redshift galaxies. However, the recent model of Gronke & Dijkstra (2014) suggests that significant Lyα enhancements can be found along particular sight lines where UV continuum photons are absorbed by dust clouds, whereas Lyα photons escape isotropically. Alternatively, Verhamme et al. (2012) have reported a strong inclination effect using Monte Carlo Lyα RT in hydrodynamical high-resolution simulations of galactic discs, in which the Lyα EW measured perpendicularly to the disc is larger than in the edge-on direction. While both UV continuum and Lyα are emitted isotropically in the disc, a fraction of the Lyα photons emitted edge-on may be scattered off by hydrogen in the face-on direction, therefore boosting the observed EW along the face-on line of sight.

Secondly, high EWs can be intrinsically produced in galaxies. For instance, Schaerer (2003) show that the EW strongly depend on the metallicity of stars and the IMF. Our SED libraries (Devriendt et al. 1999) only take into account metallicities larger than $Z = 2.10^{-3}$ so we cannot investigate the impact of metal-poor stars in our model, but we can compare the EW variation between the results from our fiducial Kennicutt IMF with a low-mass cut-off of 0.1 M$_\odot$ (labelled IMFa) and from a more top-heavy Kennicutt IMF that assumes a low-mass cut-off of 4 M$_\odot$ (IMFb). In Fig. 5 (top panel), we show the $z = 3$ model distributions of intrinsic EWs (before dust attenuation included; solid histogram), and observed EW (after dust attenuation included; dashed histogram) with IMFa. This model is in reasonable agreement with the data of Gronwall et al. (2007, blue crosses) in the range 20–70 Å, which corresponds to the peak of the EW distribution. However, the high-EW tail extending to $\sim$250 Å is poorly matched, as expected from the above discussion.[4] IMFb tends to produce higher EWs due to a larger ratio of high-mass to low-mass stars (orange dotted curve), but the distribution remains as narrow as for IMFa, and it does not reproduce the high-EW tail either. Alternative IMFs could have a stronger impact on the EW distribution, as shown by Orsi et al. (2012) who use an extreme top-heavy, flat IMF. They find a much broader EW distribution than ours, but it turns out to be even too broad compared to observations, and it peaks to higher EW than observed (see their Fig. 11). We also note that, rather than invoking very top-heavy IMFs, Forero-Romero & Dijkstra (2013) demonstrate that the stochastic sampling of the IMF can lead to strong variations in terms of EW, and significantly broaden the EW distribution.

As mentioned in Section 4.2, a starburst should be able to produce higher EWs than ongoing SF at a constant rate, as it is the case in GALICS. We test this scenario in the bottom panel of Fig. 5, where we compare the intrinsic EW distribution from our fiducial model (black solid histogram) with a modified version of GALICS in which SF has a stochastic duty cycle of 10 per cent ('stoch10'; red dashed histogram). In GALICS, SF (and all other galaxy formation processes) are integrated over timesteps of 1 Myr. Here, we randomly switch on SF once every 10 timesteps to see the effect of bursty SF on to the Lyα EWs. With this ad hoc model, we clearly see that the EW distribution is broader than the fiducial model's distribution, and agrees much better with the data of Gronwall et al. (2007).

An obvious method to mimic an SF duty-cycle is to set a high gas surface density threshold. While the criterion $\Sigma_{\rm gas}^{\rm thresh} = 10^{21}$ cm^{-2} is nearly always met in our fiducial model for galaxies considered here, we tried to increase this value to 10^{22} cm^{-2}. In this case, accreted gas needs to accumulate for longer periods in the galaxy in order to reach the surface density threshold, at least in some objects.

[3] Here, we have focused on $z = 3$ LAEs, but the issue is similar at higher redshifts, as large EW values are also measured in LAEs up to $z \approx 6$ (e.g. Kashikawa et al. 2011).

[4] It is worth pointing out here that our simulation box is few times larger than current LAE surveys, so it is unlikely that these very strong emitters are missing in our model because of our finite volume.

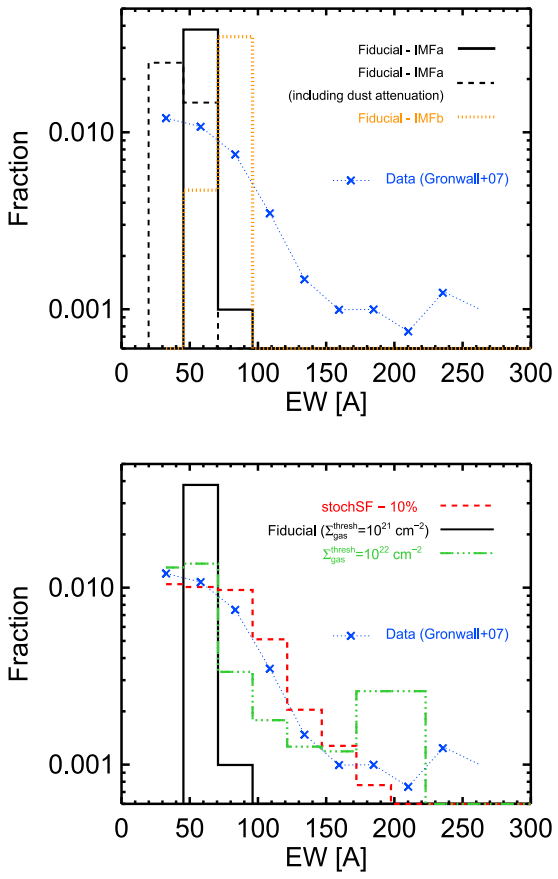

Figure 5. Lyα EWs distribution of LAEs at $z = 3$. Top: the black solid and dashed histograms show the EW distributions of LAEs predicted by our model before and after the effect of dust included, respectively. Our fiducial model assumes a Kennicutt IMF, with a low-mass cut-off of 0.1 $M_\odot$ (IMFa). For comparison, we also show the EW distribution (without dust) using a more top-heavy Kennicutt IMF, with a low-mass cut-off of 4 $M_\odot$ (IMFb; orange dotted curve). LAEs have been selected using $L_{Ly\alpha} \geq 1.2 \times 10^{42}$ erg s^{-1} and EW $\geq$ 20 Å, as in the survey of Gronwall et al. (2007, blue crosses). Bottom: to highlight the effect of starbursts on the Lyα EWs, we compare the intrinsic EW distribution from our fiducial model (solid black line), with similar models in which (i) SF occurs stochastically with a duty cycle of 10 per cent (dashed red line), and (ii) SF only occurs when the gas surface density is larger than 10^{22} cm^{-2} in galaxies (dot–dashed green line).

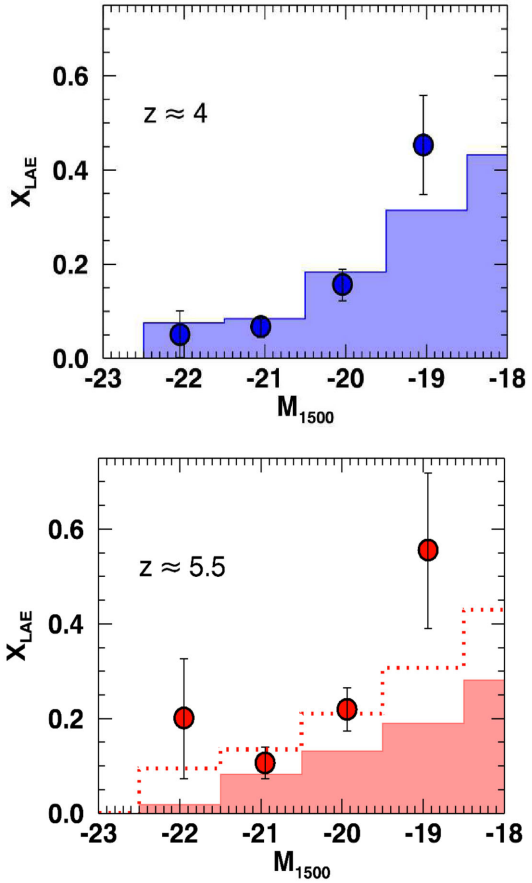

Figure 6. Fraction of strong Lyα emitters among samples of LBGs at $z \approx 4$ (top) and 5.5 (bottom). In each panel, the histogram shows the predicted fraction of LAEs X_{LAE} in five bins of rest-frame absolute UV magnitude M_{1500}. The model is compared to the data of Stark et al. (2010, represented by circles with error bars) who measured the fraction of LBGs with Lyα EWs larger than 50 Å. As shown by the dotted line in the bottom panel, we find a slightly better agreement with the observations at $z \approx 5$ with an EW cut of 45 Å instead of 50 Å (solid line).

The corresponding intrinsic EW distribution plotted as a green dot–dashed histogram on the bottom panel of Fig. 5 is similar to what we find for our ad hoc 'stoch10' model, with an extended tail towards high large EW values. Although SF occurs more rarely in these two models than in our fiducial one, we note that the intrinsic Lyα and UV LFs (and the stellar mass functions) are not changed by a large amount. Indeed, more gas accumulates in the galaxy for the 'stoch10' and high-Σ_{gas}^{thresh} models, so SF events turn more gas into stars at once using the Kennicutt law. These models even produce slightly larger SFRs, hence larger Lyα and UV luminosities, due to the power-law index of the Kennicutt law being greater than 1. However, the higher gas content would increase the effect of dust attenuation, as both quantities are correlated (section 2.2 in Paper I), so these models will no longer necessarily give a good match to the observed UV and Lyα LFs. Overall, stochastic SF scenarios constitute a viable mechanism to produce high Lyα EWs in high-redshift galaxies, and we will investigate these models in more details in future studies.

5 UV/LYα PROPERTIES OF LBGs

5.1 The fraction of emitters within LBGs

Spectroscopic follow-ups of LBG samples show that Lyα emission is more often detected in UV-fainter galaxies. In Fig. 6, we test our (fiducial) model against the observations of Stark et al. (2010) who found that the fraction of strong Lyα emitters (EW > 50 Å), X_{LAE}, increases from ≈7 per cent (20 per cent) at $M_{1500} = -22$ to 45 per cent (55 per cent) at $M_{1500} = -19$ for $z \approx 4$ ($z \approx 5$). We find a very similar trend at both $z \approx 4$ and 5.5, as shown by the histograms in the top and bottom panels. The agreement with the data of Stark et al. (2010, represented as circles) is excellent at $M_{1500} < -19.5$ for $z \approx 4$. At $z \approx 5.5$, the fraction of LAEs with EW > 50 Å in the model is slightly lower than the observations. However, as shown by the red dotted histogram, we find a good match to the data if we decrease the EW threshold by only 10 per cent (EW > 45 Å). The fractions predicted by our model in the faintest bin are a bit

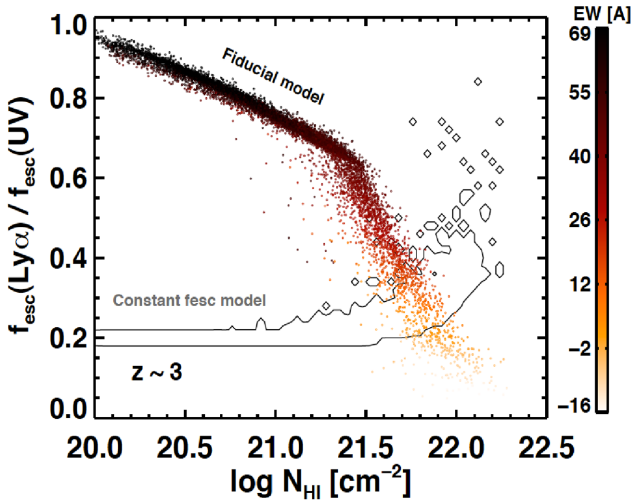

Figure 7. Lyα/UV escape fraction ratio in $z = 3$ LAEs as a function of H I shell column density. The dots represent individual galaxies in our model, colour-coded relatively to their Lyα EW (after applying dust attenuation). For comparison, we show the Lyα/UV escape fraction ratio expected from constant Lyα escape fraction models (Le Delliou et al. 2005; Nagamine et al. 2010), assuming $f_{\rm esc}({\rm Ly}\alpha) = 20$ per cent (contours).

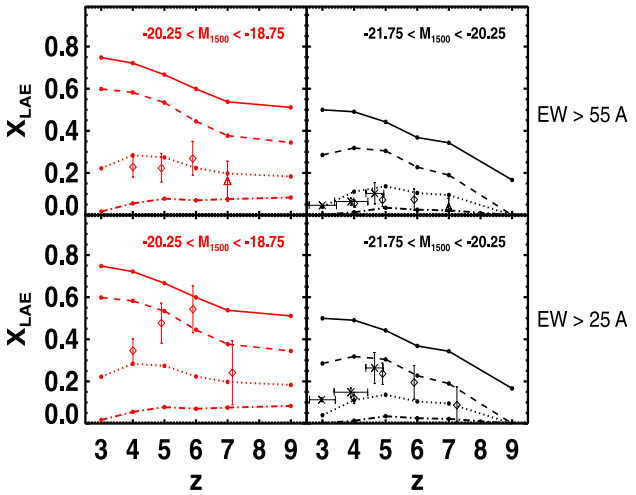

Figure 8. Fraction of Lyα emitters, $X_{\rm LAE}$, as a function of redshift among samples of faint LBGs ($-20.25 < M_{1500} < -18.75$; left-hand panels, in red) and bright LBGs ($-21.75 < M_{1500} < -20.25$; right-hand panels, in black). We show the observed fraction of strong Lyα emitters (EW $\geq$ 55 Å) and weaker emitters (EW $\geq$ 25 Å) in the top and bottom panels, respectively. Data: crosses (Cassata et al. 2015), diamonds (Stark et al. 2011; Schenker et al. 2012), and triangles (Ono et al. 2012). In all panels, we compare the observations to the LAE fraction predicted by our model for various EW cuts (solid line: EW $\geq$ 25 Å; dashed line: EW $\geq$ 35 Å; dotted line: EW $\geq$ 45 Å; dot–dashed line: EW $\geq$ 55 Å).

lower than their observational measurement, but the error bars are significant at this magnitude.

The $X_{\rm LAE}$ evolution as a function of M_{1500} is related to the anticorrelation between Lyα EW and UV magnitude which is commonly observed in LBGs and LAEs (Ando et al. 2006; Stanway et al. 2007; Ouchi et al. 2008). As discussed in Paper I, we find that UV faint galaxies are slightly more likely to display high intrinsic EW than bright LBGs. However, the main driver of the observed $X_{\rm LAE}$–M_{1500} relation in our model remains the differential dust attenuation experienced by Lyα and UV photons, caused by Lyα resonant scattering in H I gas. This is illustrated on Fig. 7, where we plot the ratio of UV to Lyα escape fractions as a function of the shell H I column density, $N_{\rm H\,I}$, for galaxies at $z = 3$ which have $L_{{\rm Ly}\alpha} > 10^{42}$ erg s^{-1}. Each dot represents a galaxy, colour-coded as a function of its Lyα EW. The $f_{\rm esc}({\rm Ly}\alpha)/f_{\rm esc}({\rm UV})$ ratio is approximatively one at low column density, but it sharply decreases towards larger values, which highlights the stronger effect of dust on Lyα due to resonant scattering in H I optically thick media. High-SFR galaxies (i.e. UV-bright galaxies) having a larger H I column density on average in GALICS, the $N_{\rm H\,I}$-dependent $f_{\rm esc}({\rm Ly}\alpha)/f_{\rm esc}({\rm UV})$ ratio unavoidably leads to a lower Lyα fraction in bright LBGs compared to faint LBGs (Fig. 6).

For comparison, we have overlaid on Fig. 7 the predictions for the constant Lyα escape fraction model (contours), which is often used in the literature to fit the observed Lyα LFs (e.g. Le Delliou et al. 2005; Nagamine et al. 2010). Fixing $f_{\rm esc}({\rm Ly}\alpha) = 20$ per cent, which is the value needed to roughly match the bright end of the $z = 3$ LF in our model, the $f_{\rm esc}({\rm Ly}\alpha)/f_{\rm esc}({\rm UV})$ ratio increases towards large $N_{\rm H\,I}$ values. A consequence of this trend, opposite to what is found with our fiducial model, would be to predict a higher LAE fraction in brighter LBGs, at odds with the observations.

The scaling of the ratio of UV continuum escape fraction to resonant Lyα escape fraction with $N_{\rm H\,I}$ and SFR, is then a key factor to explain the $X_{\rm LAE}$–M_{1500} trend, as also reported by Forero-Romero et al. (2012), who coupled hydrodynamical simulations with Lyα RT in galaxies approximated as dusty slabs.

5.2 The evolution of the Lyα fraction in LBGs with redshift

According to recent studies, the fraction of strong Lyα emitters among LBGs, $X_{\rm LAE}$, seems to increase from $z \approx 3$ to 6 (Stark, Ellis & Ouchi 2011; Cassata et al. 2015). This trend appears to invert at $z = 7$, as reported by Ono et al. (2012) and Schenker et al. (2012) who find that $X_{\rm LAE}$ dramatically drops between $z \approx 6$ and 7 (see also Pentericci et al. 2011). The redshift evolution of $X_{\rm LAE}$ could be due to a rise of the mean internal Lyα escape fraction from galaxies at $z \approx 3$–6, and by a sharp increase of neutral IGM opacity at $z \gtrsim 6$. None the less, it remains plausible that the apparent trend of the fraction of emitters in LBGs with redshift is also (i) affected, or even driven, by the intrinsic evolution of the Lyα, UV, ionizing properties of galaxies (Dayal & Ferrara 2012; Dijkstra et al. 2014), (ii) due to a reduction of the Lyα transmission caused by the increase of the number of Lyman limit systems at the end of the epoch of reionization (Bolton & Haehnelt 2012), and/or (iii) altered by small number statistics (see Dijkstra 2014; Mesinger et al. 2015, for a more detailed discussion).

Even though the study of reionization is out of the scope of this paper, it is interesting to compare our predictions to the observed redshift evolution of $X_{\rm LAE}$ without taking the effect of IGM into account. Fig. 8 shows the evolution of $X_{\rm LAE}$ of faint (in red) and bright LBGs (in black). The symbols are observational estimates of $X_{\rm LAE}$ where an LAE is defined as having EW > 55 Å in the top panels, and EW > 25 Å in the bottom panels. The solid, dashed, dotted and dot–dashed curves are predictions from our model for several EW cuts: EW $\geq$ 25 Å, EW $\geq$ 35 Å, EW $\geq$ 45 Å, and EW $\geq$ 55 Å, respectively. In all panels, we clearly see that the LAE fraction is reduced at all redshifts when higher EW cuts are applied. There is a decreasing trend with redshift for EW $\geq$ 25 Å, but it flattens for higher EW cuts.

From the upper panels (EW > 55 Å), we see that we need to lower the EW cut from 55 to 45 Å to match the data (dotted lines).

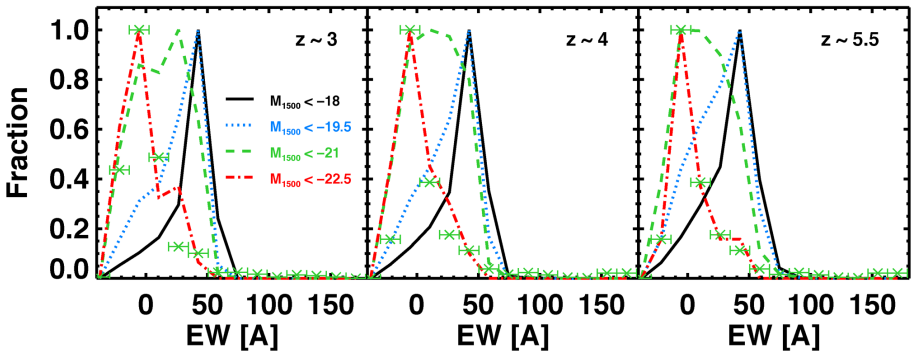

Figure 9. Lyα EWs distributions of UV-selected galaxies at $z = 3$ (left), $z = 4$ (centre), and $z = 5.5$ (right). In each panel, we show the distributions for different UV magnitude cuts, as labelled. The green crosses correspond to the data of Cassata et al. (2015, rebinned) for galaxies selected with $M_{1500} \lesssim -21$ (see their fig. 1).

In this case, the $X_{\rm LAE}$ computed from the model is based on small statistics because there are few LBGs in the corresponding ranges of magnitude with EW $\geq$ 55 Å, so it is hard to draw robust conclusions from our model. For the EW $\geq$ 25 Å measurements however (bottom panels), a better agreement is obtained if we increase the threshold to select only emitters stronger than EW = 35 Å.

In order to clarify the disagreement between the model and the observed redshift evolution of $X_{\rm LAE}$ in LBGs, as well as the strong variation with the EW cuts, we now investigate the variation of the Lyα EW distributions with UV magnitude. Indeed, by construction, should the model perfectly match the observed EW distributions of UV-selected galaxies, the redshift evolution of the LAE fraction in LBGs would be recovered. These are shown in Fig. 9 for $z = 3$, 4, and 5.5 as a function of M_{1500}, and compared to the VUDS data of Cassata et al. (2015, green crosses).

First, we note that the model distributions shift to low EW values as brighter and brighter LBGs are considered. They span a range similar to the observed ones, from ≈−40 to 70 Å. Unlike LAE surveys, which preferentially pick up low-continuum sources, UV-selected galaxies show very few high EWs ($\gtrsim$70 Å). Interestingly, the tail of the distributions appears to be slightly shifted to larger EW values for fainter LBGs. This explains why the fraction of galaxies with EW > 50 Å is found to increase towards faint UV magnitude in Fig. 6, in agreement with the data of Stark et al. (2010). However, the fraction of galaxies drops sharply at EW ≈ 50 Å for all UV magnitude selections considered here, echoing the rapid variation of $X_{\rm LAE}$ for Lyα EW thresholds near 50 Å, as discussed in Fig. 8.

Secondly, the VUDS EW distributions computed for galaxies with $M_{1500} \lesssim -21$ peak to lower EWs than the model distributions for the same UV magnitude range (green dashed curves), which is the reason why we find larger $X_{\rm LAE}$ than what is observed for EW $\geq$ 25 Å (bottom panels of Fig. 8). However, the EW distributions of Cassata et al. (2015) agree very well with the brightest LBGs in the model ($M_{1500} < -22.5$), as shown by the red dot–dashed curves.

Although our model catches well the trend between Lyα EWs and UV magnitude, the above study suggests that the exact scaling between these quantities is very sensitive to the cuts used to compute the Lyα fractions in LBGs. In addition, some fine-tuning of the model is required to fully reproduce the observed UV/Lyα cross-properties. In particular, the ratio of UV/Lyα escape fraction is found to have the right scaling with relevant physical properties, like H I column density, or SFR, in order to interpret the link between the observed properties of LAEs and LBGs, but a stronger differential UV/Lyα dust extinction in UV-bright objects is needed to improve the quantitative agreement with the data.

6 HOST HALOES OF LAEs/LBGs

In this section, we analyse the properties of the host haloes of LAEs and LBGs as predicted by our model. While the study of the clustering of LAEs and LBGs will be addressed in a companion paper (Garel et al., in prepartion), here, we focus on the halo masses and halo occupation of LAEs and LBGs as a function of redshift to identify how these galaxies, respectively, trace the dark matter structures. We also briefly discuss how the dynamical range probed by LAEs depends on the EW selection.

6.1 Halo masses as a function of Lyα /UV luminosities

On the one hand, clustering analysis reveal that LAEs reside in rather low-mass haloes, with a median mass of $\sim 10^{11}$ M$_\odot$ at $z \approx 3$ (Gawiser et al. 2007). Overall, the measured biases of LAEs at $z \approx$ 3–7 correspond to dark matter haloes in the range $M_{\rm h} = 10^{10-12}$ M$_\odot$ (Ouchi et al. 2010). On the other hand, Hildebrandt et al. (2009) find the typical halo mass of LBGs at z = 3–5 to be $\gtrsim 10^{12}$ M$_\odot$, namely about one order of magnitude more massive than those of LAEs (Hamana et al. 2004; Ouchi et al. 2004, 2005; McLure et al. 2009). Nevertheless, large uncertainties remain in the determination of the halo masses, notably for LAEs for which the selection and the detection limit can be quite different from one survey to another. Moreover, samples of NB-selected galaxies are likely to contain significant fractions of interlopers, which lead to an underestimation of the halo mass. Correcting for such effect, Kovač et al. (2007) derive a similar bias for LAEs and LBGs at $z \approx 4$. However, they report that LAEs are 2–16 times rarer than LBGs for a given halo mass. We propose to study these considerations with our model in the next paragraphs.

In Table 1, we present the median halo masses in three bins of *observed* (i.e. dust-attenuated) Lyα luminosity and UV magnitude at redshifts $z = 3$ to 7.5 in our model. The Lyα luminosity ranges are $10^{41} < L_{\rm Ly\alpha} < 10^{42}$ erg s^{-1}, $10^{42} < L_{\rm Ly\alpha} < 10^{43}$ erg s^{-1}, and $10^{43} < L_{\rm Ly\alpha} < 10^{44}$ erg s^{-1}, and we term them faint, typical, and bright LAEs. Similarly, the notation of faint, typical, and bright LBGs will be used for galaxies with $-15.8 > M_{1500} > -18.3$, $-18.3 > M_{1500} > -20.8$, and $-20.8 > M_{1500} > -23.3$. The limit values correspond to SFRs of ∼0.08, 0.8, 8, and 80 M$_\odot$ yr^{-1} according to the expected intrinsic scaling between $L_{\rm Ly\alpha}$, M_{1500}, and SFR (see Section 4.2).

First, from inspection of Table 1, we see that the host halo mass of LAEs and LBGs increases from faint to bright luminosity/magnitude at all redshifts. This is expected because the gas

Table 1. Properties of LAEs and LBGs at $z = 3$, 3.7, 5, 6, 6.6, and 7.5 for three bins of Lyα and UV luminosity. Here, LAEs are defined to have EW > 0 Å and they are classified as faint ($10^{41} < L_{\mathrm{Ly}\alpha} < 10^{42}$ erg s^{-1}), typical ($10^{42} < L_{\mathrm{Ly}\alpha} < 10^{43}$ erg s^{-1}), and bright ($10^{43} < L_{\mathrm{Ly}\alpha} < 10^{44}$ erg s^{-1}) according to their Lyα luminosity. The faint, typical, and bright samples of LBGs are selected from their UV magnitude, $-15.8 > M_{1500} > -18.3$, $-18.3 > M_{1500} > -20.8$, and $-20.8 > M_{1500} > -23.3$, respectively. $M_{\mathrm{halo}}^{\mathrm{LAE}}$ and $M_{\mathrm{halo}}^{\mathrm{LBG}}$ give the median host halo masses of LAEs and LBGs in each subsample. The subscripts and superscripts next to each value correspond to the 10th and 90th percentiles, respectively. For each subsample (faint, typical and bright), the third row shows the ratio of the number of LAEs to the number of LBGs, $n^{\mathrm{LAE}}/n^{\mathrm{LBG}}$.

		$z = 3$	$z = 4$	$z = 5$	$z = 6$	$z = 6.6$	$z = 7.5$
Faint LAEs/LBGs	$\log(M_{\mathrm{halo}}^{\mathrm{LAE}}/\mathrm{M}_\odot)$	$10.7^{+0.8}_{-0.3}$	$10.6^{+0.6}_{-0.3}$	$10.4^{+0.4}_{-0.2}$	$10.2^{+0.4}_{-0.2}$	$10.2^{+0.4}_{-0.2}$	$10.1^{+0.4}_{-0.2}$
	$\log(M_{\mathrm{halo}}^{\mathrm{LBG}}/\mathrm{M}_\odot)$	$10.7^{+0.8}_{-0.3}$	$10.5^{+0.6}_{-0.3}$	$10.4^{+0.4}_{-0.2}$	$10.2^{+0.4}_{-0.2}$	$10.1^{+0.4}_{-0.2}$	$10.1^{+0.4}_{-0.2}$
	$n^{\mathrm{LAE}}/n^{\mathrm{LBG}}$	0.96	0.91	0.91	0.95	0.98	1.00
Typical LAEs/LBGs	$\log(M_{\mathrm{halo}}^{\mathrm{LAE}}/\mathrm{M}_\odot)$	$11.5^{+0.6}_{-0.3}$	$11.4^{+0.5}_{-0.2}$	$11.1^{+0.4}_{-0.2}$	$10.9^{+0.4}_{-0.2}$	$10.8^{+0.4}_{-0.2}$	$10.7^{+0.4}_{-0.2}$
	$\log(M_{\mathrm{halo}}^{\mathrm{LBG}}/\mathrm{M}_\odot)$	$11.4^{+0.6}_{-0.3}$	$11.3^{+0.5}_{-0.3}$	$11.0^{+0.4}_{-0.2}$	$10.9^{+0.4}_{-0.2}$	$10.8^{+0.4}_{-0.2}$	$10.8^{+0.3}_{-0.2}$
	$n^{\mathrm{LAE}}/n^{\mathrm{LBG}}$	0.71	0.67	0.72	0.67	0.64	0.66
Bright LAEs/LBGs	$\log(M_{\mathrm{halo}}^{\mathrm{LAE}}/\mathrm{M}_\odot)$	$12.2^{+0.3}_{-0.2}$	$12.1^{+0.3}_{-0.2}$	$11.8^{+0.3}_{-0.2}$	$11.7^{+0.3}_{-0.2}$	$11.5^{+0.1}_{-0.1}$	$11.4^{+0.2}_{-0.2}$
	$\log(M_{\mathrm{halo}}^{\mathrm{LBG}}/\mathrm{M}_\odot)$	$12.1^{+0.4}_{-0.3}$	$12.0^{+0.4}_{-0.2}$	$11.7^{+0.4}_{-0.2}$	$11.6^{+0.3}_{-0.2}$	$11.5^{+0.2}_{-0.1}$	$11.4^{+0.4}_{-0.2}$
	$n^{\mathrm{LAE}}/n^{\mathrm{LBG}}$	0.24	0.21	0.31	0.28	0.22	0.33

accretion rate is higher in more massive haloes, so galaxies have higher SFR, hence higher intrinsic Lyα and UV emission. Secondly, for the three luminosity/magnitude bins we defined, LAEs and LBGs inhabit very similar haloes, in agreement with the results of Kovač et al. (2007). For instance, at $z = 3$, the median halo mass is 5×10^{10} M$_\odot$ for faint LAEs/LBGs, and 1–2 $\times$ 10^{12} M$_\odot$ for bright LAEs/LBGs. This result is simply due to Lyα and UV emission being both intrinsically powered by SFR, as discussed in Section 4.2.

Although we find very similar host halo masses for LAEs and LBGs at all luminosities considered here, their occupation rate of dark matter haloes significantly evolves (see Table 1). The ratio of the number of LAEs to the number of LBGs, $n^{\mathrm{LAE}}/n^{\mathrm{LBG}}$, is about one for faint objects because, at the faint end, dust extinction has little effect so nearly all LBGs are also LAEs, and their *observed* UV magnitudes and Lyα luminosities follows the expected relation given by equation (1). At the bright end, radiative transfer effects affect more strongly the Lyα intensity than the UV so that only 20–30 per cent of bright LBGs will have a bright Lyα counterpart. In Table 1, we considered LAEs to have EW > 0 Å. If we assumed a higher EW threshold (e.g. 10–30 Å), the ratio of the number of LAEs to LBGs would still be about one for faint sources but it would be less than 20–30 per cent for bright galaxies, since UV bright sources have lower EWs than faint LBGs on average (as discussed in Fig. 9).

Several reasons can be invoked to explain why LAEs are observationally measured to be located in less massive haloes than LBGs: (i) the LAEs are selected in deeper surveys than LBGs, (ii) the LAE samples were highly contaminated, or (iii) the LAEs were selected in the tail of the EW distribution where Lyα traces a very recent starburst, so their Lyα luminosity is higher than expected for a given UV magnitude (see equation 2).

6.2 Halo occupation of LAEs and LBGs

In order to investigate how LBGs and LAEs, respectively, populate dark matter haloes, we now turn our interest to the halo occupation of UV- and Lyα-selected galaxies. Figs 10 and 11 plot the mean number of galaxies per halo, $\langle N_{\mathrm{g}} \rangle_{\mathrm{halo}}$, as a function of halo mass, for $z \approx 3$ (left-hand panels) and $z \approx 6$ (right-hand panels). The black solid curves in all panels correspond to all galaxies. While our model predicts about one galaxy per halo at low M_{h}, $\langle N_{\mathrm{g}} \rangle_{\mathrm{halo}}$ increases with halo mass and reaches about 1000 (100) in the most massive structures at $z \approx 3$ ($z \approx 6$).

Here, we again split galaxies according to their observed UV and Lyα luminosities: the thick dotted blue, dashed green and dot–dashed red curves refer to faint, typical, and bright objects, respectively. Although galaxies can form in haloes with masses $\gtrsim 2 \times 10^9$ M$_\odot$ in our simulation, we can see that there is a minimum allowed host halo mass for a given UV or Lyα luminosity threshold. For instance, almost no faint LBG ($-15.8 > M_{1500} > -18.3$) inhabit haloes less massive than 10^{10} M$_\odot$ at $z = 3$ (blue dotted curve in left-hand panel of Fig. 10). Moreover, the minimum halo mass increases towards brighter objects. Again, this is the direct consequence of the UV luminosity varying as the SFR, and the SFR being proportional to the gas accretion rate, and thus to the halo mass.

Each halo mass bin is populated by one corresponding (central) galaxy of given luminosity and by satellites which belong to a fainter population: there is one central faint LBG per halo of $\log(M_{\mathrm{h}}/\mathrm{M}_\odot) \approx 10.5$, one central typical LBG per halo of $\log(M_{\mathrm{h}}/\mathrm{M}_\odot) \approx 11.5$, and one bright LBG per halo of $\log(M_{\mathrm{h}}/\mathrm{M}_\odot) \approx 12.5$. A similar behaviour is seen for LAEs (Fig. 11), but we note that the number of bright LAEs in massive haloes is less than the number of bright LBGs. This echoes the results from Table 1 where we found that bright LAEs were rarer than bright LBGs (see Section 6.1), and this is due to the stronger effect of dust attenuation for Lyα than UV continuum which can turn intrinsically bright LAEs into much fainter objects (see Section 4.2).

Still in Fig. 11, the thin curves correspond to strong emitters only (EW > 40 Å). For faint LAEs, this criterion does not remove many objects. However, $\langle N_{\mathrm{g}} \rangle_{\mathrm{halo}}$ starts decreasing more significantly for the typical and bright samples, especially for galaxies residing in massive haloes. This indicates that massive haloes are more likely to host weak emitters (low-EW galaxies) than low-mass haloes in our model.

6.3 The bias on LAE host haloes introduced by EW cuts

As noticed in Fig. 11, selecting LAEs above a given Lyα EW especially removes galaxies in more massive haloes. Here, we

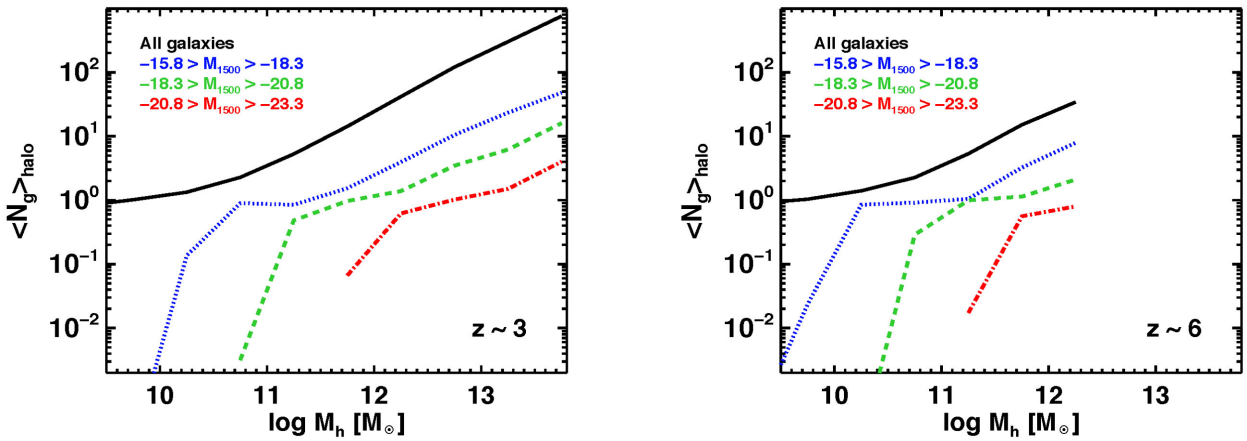

Figure 10. Halo occupation distribution of LBGs. The mean number of galaxies per dark matter halo, $\langle N_{\rm g}\rangle_{\rm halo}$, as a function of halo mass is shown by the black solid line for z =3 (left-hand panel) and $z = 6$ (right-hand panel). The coloured curves represent the mean halo occupation of faint ($-15.8 > M_{1500} > -18.3$: blue dotted line), typical ($-18.3 > M_{1500} > -20.8$: green dashed line), and bright ($-20.8 > M_{1500} > -23.3$: red dot–dashed line) LBGs.

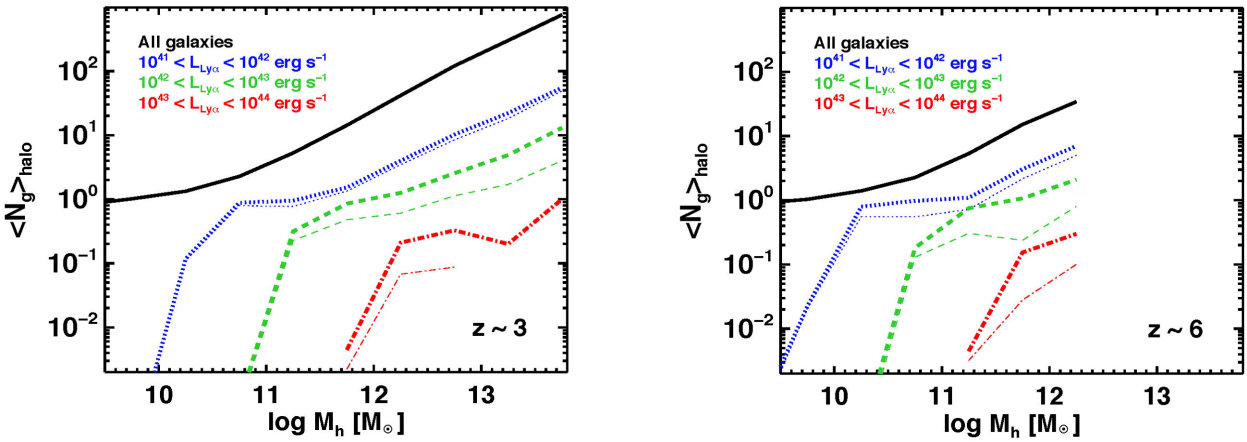

Figure 11. Halo occupation distribution of LAEs. The mean number of galaxies per dark matter halo, $\langle N_{\rm g}\rangle_{\rm halo}$, as a function of halo mass is shown by the black solid thick line for $z = 3$ (left-hand panel) and $z = 6$ (right-hand panel). The coloured thick curves represent the mean halo occupation of faint ($10^{41} < L_{{\rm Ly}\alpha} < 10^{42}$ erg s^{-1}: blue dotted line), typical ($10^{42} < L_{{\rm Ly}\alpha} < 10^{43}$ erg s^{-1}: green dashed line), and bright ($10^{43} < L_{{\rm Ly}\alpha} < 10^{44}$ erg s^{-1}: red dot–dashed line) LAEs, assuming no EW selection. The thin curves are similar but for LAEs with EW > 40 Å.

investigate this aspect more quantitatively. In Fig. 12, we plot the LAE detection rate as a function of host halo mass at $z \approx 3$ (left-hand panel) and $z \approx 6$ (right-hand panel), adopting various EW cuts. We consider only galaxies brighter than 10^{42} erg s^{-1}, and we define the LAE detection rate as the ratio of the number of LAEs with EW > 20, 35, and 50 Å (dotted, dashed and dot–dashed curves, respectively) and the number of all LAEs (i.e. galaxies with Lyα in emission, EW > 0 Å).

We find that the LAE detection rate decreases at all halo masses as the EW threshold increases. Using a value of 20 Å still allows us to detect the vast majority of LAEs. However, many line emitters may be missed when larger values are adopted according to our model. Moreover, for a given EW cut, the drop of the LAE detection rate is more significant in massive haloes than low-mass ones at both $z \approx 3$ and $z \approx 6$. As an example, for EW = 35 Å at $z \approx 3$, it decreases from ≈90 per cent at $M_{\rm h} = 10^{11}$ M$_\odot$ to 60 per cent at $M_{\rm h} = 10^{13}$ M$_\odot$. This behaviour has two main causes.

First, central, intrinsically Lyα-bright, galaxies which are located in massive haloes are often strongly affected by dust extinction which can significantly reduce, not only their Lyα luminosity, but also their EW. Secondly, the bulk of galaxies residing in massive haloes have a lower intrinsic Lyα EW than sources located in low-mass haloes in our model. They are often satellite galaxies, so they no longer accrete fresh gas from the IGM. Thus, they have less intense recent SF, which leads to lower intrinsic ratio of ionizing (i.e. Lyα) to UV-continuum photons.

Therefore, the host halo population probed by NB surveys using high-EW selections (e.g. Ouchi et al. 2008) may be biased towards low-mass haloes. Nevertheless, we remind our model does not reproduce very well the EW distributions from NB LAE surveys. As discussed in Section 4.2, we underpredict the number of high-EW sources, i.e. EW $\gtrsim$ 100–150 Å, so the curves for the LAE detection rates in Fig. 12 should be shifted up by an amount which depends on the exact form of the EW distribution. On the other hand, these high-EW sources correspond to UV-faint galaxies according to observations so they will be located in low mass haloes on average. Should they be added to our model, this could only have the effect of accentuating the trend between LAE detection rate and halo mass that we see in Fig. 12.

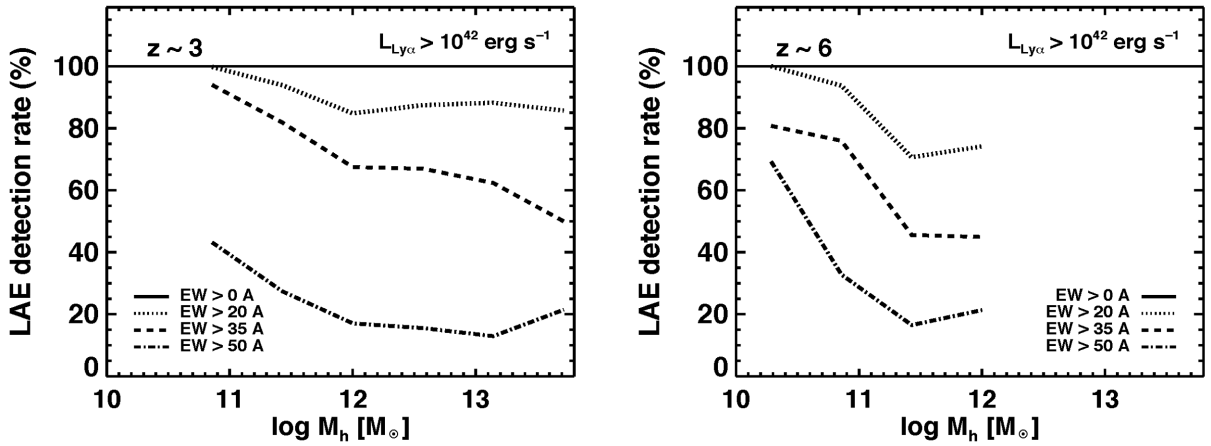

Figure 12. Detectability of LAEs as function of host halo mass for various EW thresholds for $z \sim 3$ (left-hand panel) and $z \sim 6$ (right-hand panel). The 'LAE detection rate' is the ratio of the number of LAEs with EW $>$ 20, 35, and 50 Å (dotted, dashed and dot–dashed curves, respectively) to the number of galaxies with a Lyα emission (i.e. EW $>$ 0 Å). Here, we have only considered galaxies brighter than $L_{Ly\alpha} > 10^{42}$ erg s^{-1}, which corresponds approximatively to the sensitivity limit of current photometric surveys of LAEs. Galaxies with such luminosities only inhabit haloes that are massive enough, hence the apparent cut-off of the curves at low M_h.

7 DISCUSSION AND SUMMARY

In this paper, we have investigated the connection between LAEs and LBGs from $z \approx 3$ to $z \approx 7$ with a SAM of galaxy formation. Observationally, LAEs are detected from their strong nebular Lyα emission line whereas LBG surveys pick up strong near-UV stellar continuum. While both channels intrinsically trace the stellar formation in galaxies, it remains unclear how different are the galaxies probed by these two techniques.

We have used the GALICS hybrid model to describe the formation and evolution of galaxies, based on a new high-resolution *N*-body dark matter simulation run with a set of cosmological parameters consistent with the *WMAP*-5 data release. The simulation box contains more than a billion particles in a representative volume of the Universe (100 h^{-1} cMpc on a side) which allows us to study the statistical properties of currently observed LAEs and LBGs at high-redshift. We describe the radiative transfer of Lyα and UV photons through dusty gas outflows using a simple expanding shell model. To account for the resonant scattering of Lyα photons, our model is coupled to the library of Schaerer et al. (2011a) which provides us with the Lyα escape fraction and the emergent line profile based on 3D numerical Monte Carlo RT simulations.

With this approach, we aimed at interpreting the large sets of observational constraints on LAEs and LBGs to better understand the link between these two galaxy populations. We first focused on the comparison of our model with Lyα and UV observations of Lyα- and UV-selected galaxies. In a second part, we presented predictions on the host halo masses and halo occupation of LAEs and LBGs based on our model.

We summarize the main results from our paper as follows.

(i) We can reproduce the LFs of LAEs and LBGs between $z \approx 3$ and $z \approx 7$ reasonably well. At $z \gtrsim 6$, the model may slightly underpredict the abundances of sources, as it only matches data with the lowest observed number densities. We note that the data, especially for the Lyα LFs, are not always homogeneous due to different selections and degrees of contamination, so it is not straightforward to constrain models very accurately, in particular at the highest redshifts.

(ii) Applying selection criteria similar to those used in the observations, the UV LFs of LAEs predicted by the model are in rather good agreement with the observed ones, except for LAE samples selected above high-EW thresholds. This highlights the fact that strong emitters (EW $\gtrsim$ 70 Å) are almost absent from our model, and we then investigate in more details the link between Lyα and UV emission properties of LAEs, i.e. the Lyα EWs.

(iii) While various mechanisms, extensively discussed in the literature, can produce high EWs, we suggest that bursty SF, rather than almost constant SF, should bring our model in agreement with the observed EW distributions of LAEs. We show that increasing the surface density SF threshold by an order of magnitude compared to the standard threshold can mimic stochastic SFR, needed to match the EW distributions.

(iv) We find that the fraction of strong line emitters (EW $>$ 50 Å) in LBG samples increases towards faint UV magnitudes, as reported by Stark et al. (2010) at $z = 4$–6. This trend is essentially due to resonant Lyα photons being more affected by dust than UV continuum photons in bright LBGs because these objects have a higher H I column density on average, echoing the results of Verhamme et al. (2008).

(v) We study the redshift evolution of the fraction of strong (EW $>$ 55 Å) and weak (EW $>$ 25 Å) Lyα line emitters, X_{LAE}, within UV-selected samples. Overall, X_{LAE} seems to quickly evolve when varying UV magnitude limits and Lyα EW cuts. The predictions agree reasonably well with the data for strong emitters, but the low number statistics and the rapid variation of the shape/normalization of the X_{LAE}–redshift relation with UV magnitudes limits and Lyα EW cuts prevent us from drawing robust conclusions. In addition, as shown by the study of the model EW distributions as a function of UV magnitude, a stronger differential UV/Lyα dust extinction in UV-bright objects is needed to improve the quantitative agreement with the data.

(vi) We find that LAEs and LBGs in each sample are located in very similar haloes, and that brighter sources inhabit more massive haloes average. At $z = 3$ for instance, faint LAEs and LBGs are hosted by 5×10^{10} M$_\odot$ haloes, whereas bright objects reside in haloes of $\gtrsim 10^{12}$ M$_\odot$.

(vii) The halo occupation rate of LAEs and LBGs is very similar, except for the bright sample, where LAEs appear to be about four times rarer than LBGs, in broad agreement with the observations of Kovač et al. (2007).

(viii) More massive haloes tend to host weaker Lyα emitters on average in our model, which suggests that LAEs selected with high-EW cuts will preferentially probe LAEs in low-mass haloes.

In this article, we have shown that our model can reproduce many observed statistical quantities at $z \approx 3$–7, using a rather simple modelling of galaxies and Lyα RT. Some additional ingredients may still be necessary to accommodate the tail of the EW distribution, possibly due to burstiness, and the exact scaling between UV luminosities and Lyα EW, by increasing the effect of dust in UV-bright objects. Nevertheless, within a single and coherent framework, we are able to interpret reasonably well the abundances of LAEs and LBGs, as well as the UV LFs of LAEs and the Lyα fraction in UV-selected samples.

The picture emerging from this study of the Lyα, UV, and halo properties of high-redshift galaxies is consistent with the idea that LAEs are a subset of the LBG population. The apparent differences between these two populations would simply arise from the EW selection in LAE surveys, and the continuum detection limit used to select LBGs. In other terms, LAEs undetected in the UV should always be probed by deeper LBG surveys. At given SFR, LAEs and LBGs should have very similar UV magnitude, and the effect of dust on Lyα photons will redistribute the most massive, intrinsically Lyα-bright, galaxies at fainter fluxes and lower EWs, although these can still appear as LBGs (Shapley et al. 2003). As a consequence, LAEs that are observed are more likely to have lower dust extinction than LBGs. This picture seems consistent with the comparison study of the mid-IR properties of LAEs and LBGs (Yuma et al. 2010), the work of Verhamme et al. (2008) based on stellar population and Lyα radiative transfer modelling, the hydrodynamical simulations of Dayal & Ferrara (2012), and the results of Cooke (2009) and Schaerer, de Barros & Stark (2011b) who demonstrate that the Lyα emission properties of UV-selected galaxies can be statistically inferred from broad-band photometry and SED modelling techniques (see Dunlop 2013, for a review).

None the less, LAEs remain quite powerful at probing faint (i.e. low-mass) high-redshift star-forming galaxies, especially strong emitters which would require very deep observations to be detected in UV continuum surveys. In addition, the observational and theoretical study of the Lyα line profile and morphology of LAEs hold great potential in probing the distribution, the content, and the kinematics of the gas in the ISM, but also at larger scale in the circumgalactic and intergalactic media (see e.g. Barnes, Garel & Kacprzak 2014). Increased numerical power along with larger data samples extending to fainter luminosities and higher redshift, expected from ongoing and forthcoming surveys (e.g. MUSE, HETDEX, KCWI or Hyper Suprime-Cam), will undoubtedly help refine our understanding of Lyα emitters, and galaxy formation and evolution at high redshift in general.

ACKNOWLEDGEMENTS

The authors thank the anonymous referee for useful comments that helped to improve this paper. We thank Daniel Schaerer for his helpful comments on an earlier version of the manuscript. TG is the recipient of an Australian Research Council SuperScience Fellowship. This work was granted access to the HPC resources of CINES under the allocation 2012-c2012046642 made by GENCI (Grand Equipement National de Calcul Intensif). LMD acknowledges support from the Lyon Institute of Origins under grant ANR-10-LABX-66. MH acknowledges the support of the Swedish Research Council, Vetenskapsrådet and the Swedish National Space Board (SNSB).

REFERENCES

Ahn S.-H., Lee H.-W., Lee H. M., 2001, ApJ, 554, 604
Ajiki M. et al., 2003, AJ, 126, 2091
Ajiki M. et al., 2004, PASJ, 56, 597
Ajiki M., Mobasher B., Taniguchi Y., Shioya Y., Nagao T., Murayama T., Sasaki S. S., 2006, ApJ, 638, 596
Ando M., Ohta K., Iwata I., Akiyama M., Aoki K., Tamura N., 2006, ApJ, 645, L9
Arnouts S. et al., 2005, ApJ, 619, L43
Bacon R. et al., 2006, The Messenger, 124, 5
Barnes L. A., Haehnelt M. G., Tescari E., Viel M., 2011, MNRAS, 416, 1723
Barnes L. A., Garel T., Kacprzak G. G., 2014, PASP, 126, 969
Berry M. et al., 2012, ApJ, 749, 4
Birnboim Y., Dekel A., 2003, MNRAS, 345, 349
Blanc G. A. et al., 2011, ApJ, 736, 31
Bolton J. S., Haehnelt M. G., 2012, MNRAS, p. 412
Bouwens R. J., Illingworth G. D., Franx M., Ford H., 2007, ApJ, 670, 928
Bouwens R. J., Illingworth G. D., Franx M., Ford H., 2008, ApJ, 686, 230
Bouwens R. J. et al., 2010, ApJ, 709, L133
Bouwens R. J. et al., 2011, ApJ, 737, 90
Cassata P. et al., 2011, A&A, 525, A143
Cassata P. et al., 2015, A&A, 573, A24
Castellano M. et al., 2010, A&A, 524, A28
Cattaneo A., Dekel A., Devriendt J., Guiderdoni B., Blaizot J., 2006, MNRAS, 370, 1651
Charlot S., Fall S. M., 1993, ApJ, 415, 580
Cooke J., 2009, ApJ, 704, L62
Davis M., Efstathiou G., Frenk C. S., White S. D. M., 1985, ApJ, 292, 371
Dawson S., Rhoads J. E., Malhotra S., Stern D., Wang J., Dey A., Spinrad H., Jannuzi B. T., 2007, ApJ, 671, 1227
Dayal P., Ferrara A., 2012, MNRAS, 421, 2568
Dayal P., Maselli A., Ferrara A., 2011, MNRAS, 410, 830
Dekel A. et al., 2009, Nature, 457, 451
Devriendt J. E. G., Guiderdoni B., Sadat R., 1999, A&A, 350, 381
Dijkstra M., 2014, PASA, 31, 40
Dijkstra M., Wyithe J. S. B., 2010, MNRAS, 408, 352
Dijkstra M., Wyithe J. S. B., 2012, MNRAS, 419, 3181
Dijkstra M., Haiman Z., Spaans M., 2006, ApJ, 649, 14
Dijkstra M., Wyithe S., Haiman Z., Mesinger A., Pentericci L., 2014, MNRAS, 440, 3309
Dunlop J. S., 2013, in Wiklind T., Mobasher B., Bromm V., eds, Astrophysics and Space Science Library Vol. 396, The First Galaxies. Springer-Verlag, Berlin, p. 223
Duval F., Schaerer D., Östlin G., Laursen P., 2014, A&A, 562, A52
Finkelstein S. L., Rhoads J. E., Malhotra S., Pirzkal N., Wang J., 2007, ApJ, 660, 1023
Finkelstein S. L., Rhoads J. E., Malhotra S., Grogin N., 2009, ApJ, 691, 465
Finkelstein S. L. et al., 2011, ApJ, 729, 140
Forero-Romero J. E., Dijkstra M., 2013, MNRAS, 428, 2163
Forero-Romero J. E., Yepes G., Gottlöber S., Knollmann S. R., Cuesta A. J., Prada F., 2011, MNRAS, 415, 3666
Forero-Romero J. E., Yepes G., Gottlöber S., Prada F., 2012, MNRAS, 419, 952
Gabasch A. et al., 2004, A&A, 421, 41
Garel T., Blaizot J., Guiderdoni B., Schaerer D., Verhamme A., Hayes M., 2012, MNRAS, 422, 310 (Paper I)
Gawiser E. et al., 2006, ApJ, 642, L13
Gawiser E. et al., 2007, ApJ, 671, 278
González V., Labbé I., Bouwens R. J., Illingworth G., Franx M., Kriek M., 2011, ApJ, 735, L34
Gronke M., Dijkstra M., 2014, MNRAS, 444, 1095
Gronwall C. et al., 2007, ApJ, 667, 79
Hamana T., Ouchi M., Shimasaku K., Kayo I., Suto Y., 2004, MNRAS, 347, 813
Hansen M., Oh S. P., 2006, MNRAS, 367, 979

Hatton S., Devriendt J. E. G., Ninin S., Bouchet F. R., Guiderdoni B., Vibert D., 2003, MNRAS, 343, 75
Hayes M. et al., 2010, Nature, 464, 562
Henry A. L., Martin C. L., Dressler A., Sawicki M., McCarthy P., 2012, ApJ, 744, 149
Hibon P., Kashikawa N., Willott C., Iye M., Shibuya T., 2012, ApJ, 744, 89
Hildebrandt H., Pielorz J., Erben T., van Waerbeke L., Simon P., Capak P., 2009, A&A, 498, 725
Hu E. M., Cowie L. L., McMahon R. G., 1998, ApJ, 502, L99
Hu E. M., Cowie L. L., Barger A. J., Capak P., Kakazu Y., Trouille L., 2010, ApJ, 725, 394
Inoue A. K., Shimizu I., Iwata I., Tanaka M., 2014, MNRAS, 442, 1805
Iwata I., Ohta K., Tamura N., Akiyama M., Aoki K., Ando M., Kiuchi G., Sawicki M., 2007, MNRAS, 376, 1557
Iye M. et al., 2006, Nature, 443, 186
Jose C., Srianand R., Subramanian K., 2013, MNRAS, 435, 368
Kashikawa N. et al., 2006, ApJ, 648, 7
Kashikawa N. et al., 2011, ApJ, 734, 119
Kennicutt R. C., Jr, 1983, ApJ, 272, 54
Kennicutt R. C., Jr, 1989, ApJ, 344, 685
Kennicutt R. C., Jr, 1998, ApJ, 498, 541
Kereš D., Katz N., Weinberg D. H., Davé R., 2005, MNRAS, 363, 2
Kobayashi M. A. R., Totani T., Nagashima M., 2007, ApJ, 670, 919
Kobayashi M. A. R., Totani T., Nagashima M., 2010, ApJ, 708, 1119
Komatsu E. et al., 2009, ApJS, 180, 330
Kovač K., Somerville R. S., Rhoads J. E., Malhotra S., Wang J., 2007, ApJ, 668, 15
Kulas K. R., Shapley A. E., Kollmeier J. A., Zheng Z., Steidel C. C., Hainline K. N., 2012, ApJ, 745, 33
Laursen P., Sommer-Larsen J., 2007, ApJ, 657, L69
Laursen P., Sommer-Larsen J., Andersen A. C., 2009, ApJ, 704, 1640
Laursen P., Sommer-Larsen J., Razoumov A. O., 2011, ApJ, 728, 52
Laursen P., Duval F., Östlin G., 2013, ApJ, 766, 124
Le Delliou M., Lacey C., Baugh C. M., Guiderdoni B., Bacon R., Courtois H., Sousbie T., Morris S. L., 2005, MNRAS, 357, L11
Lee K.-S., Giavalisco M., Gnedin O. Y., Somerville R. S., Ferguson H. C., Dickinson M., Ouchi M., 2006, ApJ, 642, 63
McLinden E. M. et al., 2011, ApJ, 730, 136
McLure R. J., Cirasuolo M., Dunlop J. S., Foucaud S., Almaini O., 2009, MNRAS, 395, 2196
McLure R. J., Dunlop J. S., Cirasuolo M., Koekemoer A. M., Sabbi E., Stark D. P., Targett T. A., Ellis R. S., 2010, MNRAS, 403, 960
Madau P., 1995, ApJ, 441, 18
Madau P., Pozzetti L., Dickinson M., 1998, ApJ, 498, 106
Malhotra S., Rhoads J. E., 2004, ApJ, 617, L5
Mao J., Lapi A., Granato G. L., de Zotti G., Danese L., 2007, ApJ, 667, 655
Mathis J. S., Mezger P. G., Panagia N., 1983, A&A, 128, 212
Mesinger A., Aykutalp A., Vanzella E., Pentericci L., Ferrara A., Dijkstra M., 2015, MNRAS, 446, 566
Murayama T. et al., 2007, ApJS, 172, 523
Nagamine K., Ouchi M., Springel V., Hernquist L., 2010, PASJ, 62, 1455
Neufeld D. A., 1990, ApJ, 350, 216
Neufeld D. A., 1991, ApJ, 370, L85
Oesch P. A. et al., 2010, ApJ, 709, L16
Oesch P. A. et al., 2012, ApJ, 759, 135
Ono Y., Ouchi M., Shimasaku K., Dunlop J., Farrah D., McLure R., Okamura S., 2010, ApJ, 724, 1524
Ono Y. et al., 2012, ApJ, 744, 83
Orsi A., Lacey C. G., Baugh C. M., 2012, MNRAS, 425, 87
Osterbrock D. E., Ferland G. J., 2006, Astrophysics of Gaseous Nebulae and Active Galactic Nuclei. University Science Books, Mill Valley, CA
Ouchi M. et al., 2003, ApJ, 582, 60
Ouchi M. et al., 2004, ApJ, 611, 685
Ouchi M. et al., 2005, ApJ, 635, L117
Ouchi M. et al., 2008, ApJS, 176, 301
Ouchi M. et al., 2009, ApJ, 706, 1136
Ouchi M. et al., 2010, ApJ, 723, 869
Pentericci L. et al., 2011, ApJ, 743, 132
Pirzkal N., Malhotra S., Rhoads J. E., Xu C., 2007, ApJ, 667, 49
Rauch M. et al., 2008, ApJ, 681, 856
Reddy N. A., Steidel C. C., Pettini M., Adelberger K. L., Shapley A. E., Erb D. K., Dickinson M., 2008, ApJS, 175, 48
Rhoads J. E., Malhotra S., Dey A., Stern D., Spinrad H., Jannuzi B. T., 2000, ApJ, 545, L85
Santos M. R., 2004, MNRAS, 349, 1137
Sawicki M., Thompson D., 2006, ApJ, 648, 299
Schaerer D., 2003, A&A, 397, 527
Schaerer D., Hayes M., Verhamme A., Teyssier R., 2011a, A&A, 531, A12
Schaerer D., de Barros S., Stark D. P., 2011b, A&A, 536, A72
Schenker M. A., Stark D. P., Ellis R. S., Robertson B. E., Dunlop J. S., McLure R. J., Kneib J.-P., Richard J., 2012, ApJ, 744, 179
Shapley A. E., Steidel C. C., Adelberger K. L., Dickinson M., Giavalisco M., Pettini M., 2001, ApJ, 562, 95
Shapley A. E., Steidel C. C., Pettini M., Adelberger K. L., 2003, ApJ, 588, 65
Shibuya T., Kashikawa N., Ota K., Iye M., Ouchi M., Furusawa H., Shimasaku K., Hattori T., 2012, ApJ, 752, 114
Shimasaku K. et al., 2006, PASJ, 58, 313
Shioya Y. et al., 2009, ApJ, 696, 546
Spergel D. N. et al., 2007, ApJS, 170, 377
Springel V., 2005, MNRAS, 364, 1105
Stanway E. R. et al., 2007, MNRAS, 376, 727
Stark D. P., Ellis R. S., Chiu K., Ouchi M., Bunker A., 2010, MNRAS, 408, 1628
Stark D. P., Ellis R. S., Ouchi M., 2011, ApJ, 728, L2
Steidel C. C., Giavalisco M., Pettini M., Dickinson M., Adelberger K. L., 1996, ApJ, 462, L17
Steidel C. C., Adelberger K. L., Giavalisco M., Dickinson M., Pettini M., 1999, ApJ, 519, 1
Steidel C. C., Adelberger K. L., Shapley A. E., Pettini M., Dickinson M., Giavalisco M., 2003, ApJ, 592, 728
Steidel C. C., Erb D. K., Shapley A. E., Pettini M., Reddy N., Bogosavljević M., Rudie G. C., Rakic O., 2010, ApJ, 717, 289
Taniguchi Y. et al., 2005, PASJ, 57, 165
Tasitsiomi A., 2006, ApJ, 645, 792
Tweed D., Devriendt J., Blaizot J., Colombi S., Slyz A., 2009, A&A, 506, 647
van Breukelen C., Jarvis M. J., Venemans B. P., 2005, MNRAS, 359, 895
Vanzella E. et al., 2011, ApJ, 730, L35
Venemans B. P. et al., 2005, A&A, 431, 793
Verhamme A., Schaerer D., Maselli A., 2006, A&A, 460, 397
Verhamme A., Schaerer D., Atek H., Tapken C., 2008, A&A, 491, 89
Verhamme A., Dubois Y., Blaizot J., Garel T., Bacon R., Devriendt J., Guiderdoni B., Slyz A., 2012, A&A, 546, A111
Wang J., Malhotra S., Rhoads J. E., Zhang H., Finkelstein S. L., 2009, ApJ, 706, 762
Yajima H., Li Y., Zhu Q., Abel T., 2012, MNRAS, 424, 884
Yuma S., Ohta K., Yabe K., Shimasaku K., Yoshida M., Ouchi M., Iwata I., Sawicki M., 2010, ApJ, 720, 1016
Zheng Z., Miralda-Escudé J., 2002, ApJ, 578, 33

This paper has been typeset from a TEX/LATEX file prepared by the author.